T-4666

BUCKLING OF DRILLPIPE IN A CURVED BOREHOLE

by

Joe Morgan

T-4666

A thesis submitted to the faculty and the Board of Trustees of the Colorado School of Mines in partial fulfillment of the requirements for the degree of Master of Science (Petroleum Engineering).

Golden, Colorado

Date Aug. 30, 1995

Signed: _____

Joe Morgan

Approved: _____ 8/30/95

Dr. Bill J. Mitchell
Thesis Advisor

_____

Dr. Craig W. Van Kirk
Professor and Head,
Department of Petroleum Engineering

ABSTRACT

A laboratory apparatus was constructed for measuring the buckling loads of a rod constrained inside a plastic tube. Buckling experiments were conducted with curved and straight outer tubes that constrained the rod. The buckling behavior was observed and discussed. The data is presented in graphical form as load-displacement curves as well as in tabular form. The buckling loads and displacements are compared with the solutions to the buckling equations of Euler, Dawson and Paslay, Chen et. al., and Suryanarayana and McCann. Derivations are presented of Euler, Paslay and Bogy, Dawson and Paslay, Lubinski, Chen et. al., Juvkam-Wold et. al., and Suryanarayana and McCann.

TABLE OF CONTENTS

LIST OF FIGURES

LIST OF TABLES

ACKNOWLEDGMENTS

The author expresses his gratitude to Dr. Bill Mitchell, Thesis Advisor, whose guidance and encouragement were felt throughout this thesis. His insights into the buckling phenomenon were invaluable. Thanks also to Jorge Sampaio who provided an intuitive feel for the buckling process. Gratitude is also extended to Dr. Richard Christiansen and Professor Don Dickinson for serving on my graduate committee. I also wish to thank my spouse, Jana, whose hard work and infinite patience have made my education possible.

DEDICATION

This thesis is dedicated to my father, Tim Morgan, who nurtured my curiosity.

INTRODUCTION

In coiled tubing operations and in the drilling of extended reach or horizontal wells, limitations exist because of the buckling of tubulars. Buckling can result in lock-up where any additional slack-off weight would not be transmitted to the drill bit or packer but into lateral forces between the pipe and wellbore.

Euler showed that buckling takes place when the compressive load on a bar exceeds the critical buckling load. Upon loading, before Euler buckling is initiated, the axial force increases linearly with the displacement. At this point the bar is bent. Once the critical Euler buckling load is reached large displacements result with little increase in axial load. A sharp change in slope results on the load-displacement curve and it is this change in slope that defines Euler buckling.

However, unlike Euler buckling, in oil field operations the buckling of tubulars is laterally constrained by the wall of the wellbore. The buckling proceeds through two stages: sinusoidal buckling, then helical buckling. With slack-off (compressive load) a lateral deflection forms a sinusoidal shape along the bottom of the borehole. As with Euler buckling, the critical buckling load for sinusoidal buckling is where a sharp change in slope occurs on the load-displacement curve.

Further increase in the compressive load causes the amplitude of the sinusoidal shape to increase and the tubular begins to "climb" the side of the borehole. When the critical load for helical buckling is reached (again, where the change in slope occurs on the load-displacement curve), the tubular has formed a helix that is in full contact with the wall of the wellbore.

After sinusoidal buckling is initiated, most of the increase in the slack-off weight is used to increase the amplitude of the sinusoidal shape. Once the helical shape is formed, most of the increase in the slack-off weight is transmitted into lateral forces against the wall of the wellbore. This increasing lateral load results in increasing friction and drag and eventual lock-up. Any further increase in slack-off weight is no longer transmitted to the bit at the other end.

Avoiding buckling and subsequent lock-up is significant in designing and planning wells. Mathematical expressions for sinusoidal and helical buckling loads have been developed in several works; however, all of these expressions were derived for straight boreholes. In practice, boreholes are seldom straight. In this paper, experiments were conducted to simulate buckling in a horizontal borehole with varying curvature. Data was collected with borehole curvature ranging from straight to a dogleg severity of 65°/100 ft.

THEORY

Euler Buckling

Euler[1] developed the well known equation which relates column material and geometry to the critical buckling load

$$F_{\alpha} = \frac{\pi^2 EI}{L^2} \tag{1}$$

The quantity F_{cr} is the critical buckling load that puts the column in a condition of unstable equilibrium. In this state, any slight movement of the support or small increase in the load will cause the column to buckle. Of course, a drill string in a borehole is not classified as an Euler column since it is constrained laterally by the borehole wall. However, Euler's F_{cr} will be used in this paper for comparison purposes.

Sinusoidal Buckling

When the axial load reaches a critical value, sinusoidal buckling occurs along the bottom of the borehole. As the load increases, the amplitude of the sine wave increases and the waves begin to climb the wall of the borehole.

The first theoretical work for buckling of a rod in a horizontal cylinder was done by Paslay and Bogy[2]. Their formula for the critical axial load for n-th order sinusoidal buckling is

$$F_{cr(n)} = (1-\nu)\overline{E}I\frac{\pi^2}{L^2}\left(n^2 + \frac{1}{n^2}\frac{L^4 \rho A g}{\pi^4 \overline{E} I R}\right) \tag{2}$$

where

$$\overline{E} = \frac{(1-\nu)E}{(1+\nu)(1-2\nu)} \tag{3}$$

Equation (2) was modified by Dawson and Paslay[3] to

$$F_{cr(n)} = \frac{(1-\nu)^2}{(1+\nu)(1-2\nu)} EI \frac{\pi^2}{L^2}\left(n^2 + \frac{L^4 \rho Ag}{n^2 \pi^4 EIR}\right) \tag{4}$$

Suryanarayana and McCann[4] showed that this modification can be made only by neglecting the lateral strain due to Poisson's ratio. This allows the $\overline{E}$ in the denominator in equation (2) to be replaced with E.

The term $\rho Ag/R$ in equation (4) is the modulus of the foundation and represents the resistance to buckling offered by the foundation, or in this case, the borehole. It is easily seen that as $\rho Ag/R \rightarrow \infty$ the buckling load, $F_{cr(n)}$, approaches ∞, and as $\rho Ag/R \rightarrow 0$ equation (4) reduces to the classical Euler equation.

The critical buckling load is the smallest value for $F_{cr(n)}$ given by equation (4). The value of n that minimizes $F_{cr(n)}$ is arrived at in different ways. Dawson and Paslay found the minimizing value of n by treating n as a continuous variable and solving

$$\frac{\partial F_{cr(n)}}{\partial n} = 0 \tag{5}$$

which yields

$$n = \frac{L}{\pi}\left(\frac{\rho Ag}{EIR}\right)^{1/4} \tag{6}$$

When this is substituted back into equation (4) the critical buckling load results

$$F_{cr} = 2\sqrt{\frac{EI\rho Ag}{R}} \tag{7}$$

Equation (7) is the minimum load required to initiate sinusoidal buckling as derived by Dawson and Paslay.

Suryanarayana and McCann showed that since equation (6) does not always yield an integer value for n, equation (7) actually predicts a lower bound for F_{cr}. This critical force does not reduce to the classical Euler equation as $\rho Ag/R \rightarrow 0$ and this could lead to erroneous results for short rods.

Suryanarayana and McCann suggest rounding the n calculated with equation (6) to the next largest and smallest integer values (if $n<1$ then use only the next largest integer).

These integer values are then used to calculate F_{cr} using equation (4) and the smallest F_{cr} that results is the actual critical buckling load.

The data collected in this paper will be compared to the calculated F_{cr} values using Euler's equation (1), Dawson and Paslay's equation (7), and the method suggested by Suryanarayana and McCann, using equations (4) and (6).

Helical Buckling

As the axial load increases the sinusoidally buckled rod climbs the wall of the borehole until a helix results. A fully developed helix occurs when the rod "corkscrews" once around the wall of the borehole.

Lubinski, Althouse, and Logan[5] found the relationship between axial load and helical pitch, equation (A66), that is the foundation for the derivation of the critical helical buckling load. Chen, Lin, and Cheatham[6] used energy methods to derive the nth order critical buckling load for helical buckling

$$F_{hel(n)} = 4EI\frac{\pi^2}{L^2}\left(n^2 + \frac{1}{n^2}\frac{L^4 \rho Ag}{8\pi^4 EIR}\right) \tag{8}$$

The value of n that minimizes $F_{hel(n)}$ is given by

$$n = \frac{L}{\pi}\left(\frac{\rho Ag}{8EIR}\right)^{1/4} \tag{9}$$

Substituting equation (9) into equation (8) yields the critical buckling load for helical buckling

$$F_{hel} = 2\sqrt{2}\sqrt{\frac{EI\rho Ag}{R}} \tag{10}$$

If the substitution $p=L/n$ is made into equation (8), then $F_{hel(n)}$ reduces to F given by Lubinski in equation (A66).

Suryanarayana and McCann suggest using the same method for equations (8) and (9) as used for sinusoidal buckling. That is, equation (10) only predicts the lower bound for F_{hel}, and equation (8) must be used to avoid erroneous results.

The data collected in this paper will be compared to the calculated F_{hel} given by Chen's equation (10) and by using Suryanarayana's method with equations (8) and (9).

EXPERIMENTAL STUDY

Experimental Apparatus

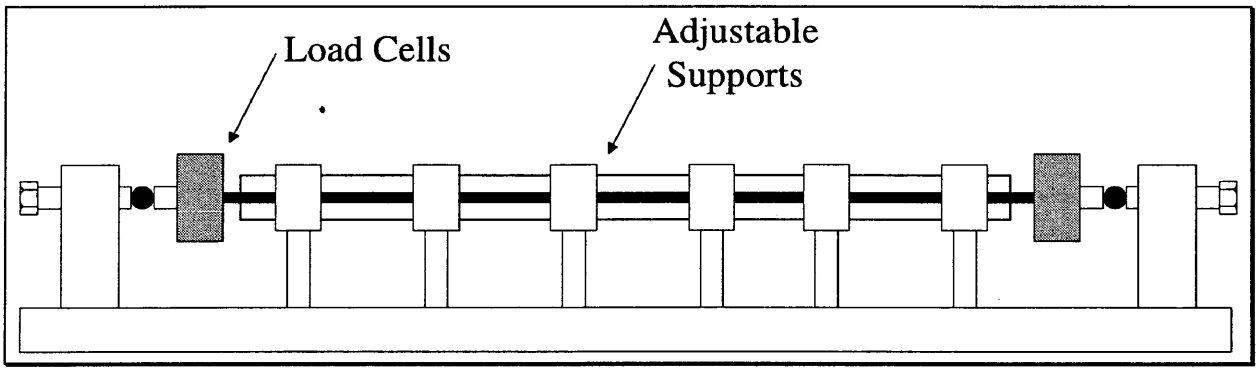

Figure 1. Schematic diagram of experimental apparatus.

The experimental apparatus consists of a clear polycarbonate tube with an aluminum rod on the inside. A schematic diagram is shown in Figure 1. Rods of 1/4 in. diameter were buckled inside the 3/4 in. ID tube. The plastic tube is supported such that vertical and horizontal adjustments can be made at one-foot intervals. There is a load cell placed in-line at both ends of the rod, and the ends of the rod are constrained by a spherical ball joint. Buckling takes place by manually turning a load screw at either end of the rod. The curvature of the "borehole" can be varied by pushing the plastic rod up or down with the adjustable supports. Axial displacement is measured at the end with a Vernier caliper.

The load cells are conventional strain gage load cells manufactured by Houston Scientific International. The range of the load cells are 0-1200 lbs which corresponds to 0-10 mV with 5V excitation. Excitation is provided by a stable 5V supply with digital display manufactured by Newport. The overall calibrated accuracy is estimated to be ±0.5 lbs which is determined by the accuracy of the calibration weights. The Vernier caliper is used to manually measure the displacement with an accuracy of ±0.0005 in. Detailed figures of the experimental apparatus are shown in the appendix.

Experimental Procedure

Before each experiment, the inside of the borehole and the aluminum rod specimen are cleaned with a commercial solvent, inspected for any damage, then lightly lubricated. The adjustable supports are moved both horizontally and vertically until the plastic borehole is aligned straight between the two ball joints at each end. The rod specimen is then placed inside the tube and seated into the load cells. The supports are adjusted again in the vertical direction so that the rod is lying on the bottom of the borehole. Care was taken to ensure that the borehole remained as straight as possible. The loading screws were turned in until they just made contact, and this zero displacement position was measured using the calipers.

The loading screw at one end, the moving end, is turned to provide displacement intervals of approximately 0.001 in. (the other non-moving end is referred as the stationary end). The displacement at the moving end is measured using the calipers and this data recorded along with the voltage and loads from each of the load cells. The onset of sinusoidal buckling was visually observed and noted. The onset of helical buckling and any "snapping" (see the Results section) was also noted. Once a maximum load was reached, the rod was unloaded and the data recorded while the rod un-buckled.

The adjustable supports in the center of the apparatus were then raised or lowered to a predetermined height for a specific borehole curvature, or dogleg severity. The cycle of buckling and un-buckling was repeated for the curved borehole.

RESULTS

Suryanarayana and McCann defined a reverse helix as a helix that reverses its direction halfway along its length. As the load is increased, a snap occurs, sometimes with a loud, audible snap, that removes the reverse helix. They reported that snapping is the result of frictional effects between the rod and the wall of the outer tube. When snapping occurs a load reversal results in which there is a sudden decrease in load without a change in the displacement.

Observations and data in this paper confirm the snapping as well as the effects of friction on this phenomenon. With the absence of lubrication, the snapping is much more audible and "violent" than when the OD of the rod is lubricated. Observations also indicate that snapping is rate sensitive. That is, if the buckling load is applied at a rate such that the rod rapidly progresses from sinusoidally buckled to helically buckled the snapping is much more audible and "violent." With a straight borehole, a reverse helix always occurs and some degree of snapping always removes the reversal. However, the reversal is not removed in the loading process but in the unloading process. That is, the rod is never helically buckled along its entire length during loading.

The expected critical buckling loads for sinusoidal buckling were calculated for each rod diameter and are shown in Table 1. The expected critical buckling loads for helical buckling are shown in Table 2.

Rod Diameter (in)	Euler F_{cr} (lb)	Dawson & Paslay F_{cr} (lb)	Suryanarayana F_{cr} (lb)
0.25	0.01	7.69	7.70
0.375	0.03	27.38	45.12

Table 1. Expected critical buckling loads for sinusoidal buckling.

Rod Dia(in)	Chen F_{hel} (lb)	Suryanarayana F_{hel} (lb)
0.25	10.87	16.62
0.375	38.66	78.98

Table 2. Expected critical buckling loads for helical buckling.

Buckling in a Straight Borehole

A typical curve for loading and unloading in a straight borehole is shown in Figure 2. Once the rod is buckled, the sine waves grow in amplitude and "climb" the wall of the borehole (A to B) until a snap occurs and a helix is formed at the stationary end. At this point, a sine wave exists along half the length of the rod and a helix along the other half (see Figure 3). As the load is increased, the sine wave continues to climb the wall (B to C) and the pitch of the helix shortens slightly. The sine wave eventually forms a helix in the opposite direction of the existing helix. This helix reversal persists throughout the remainder of the loading process (C to D).

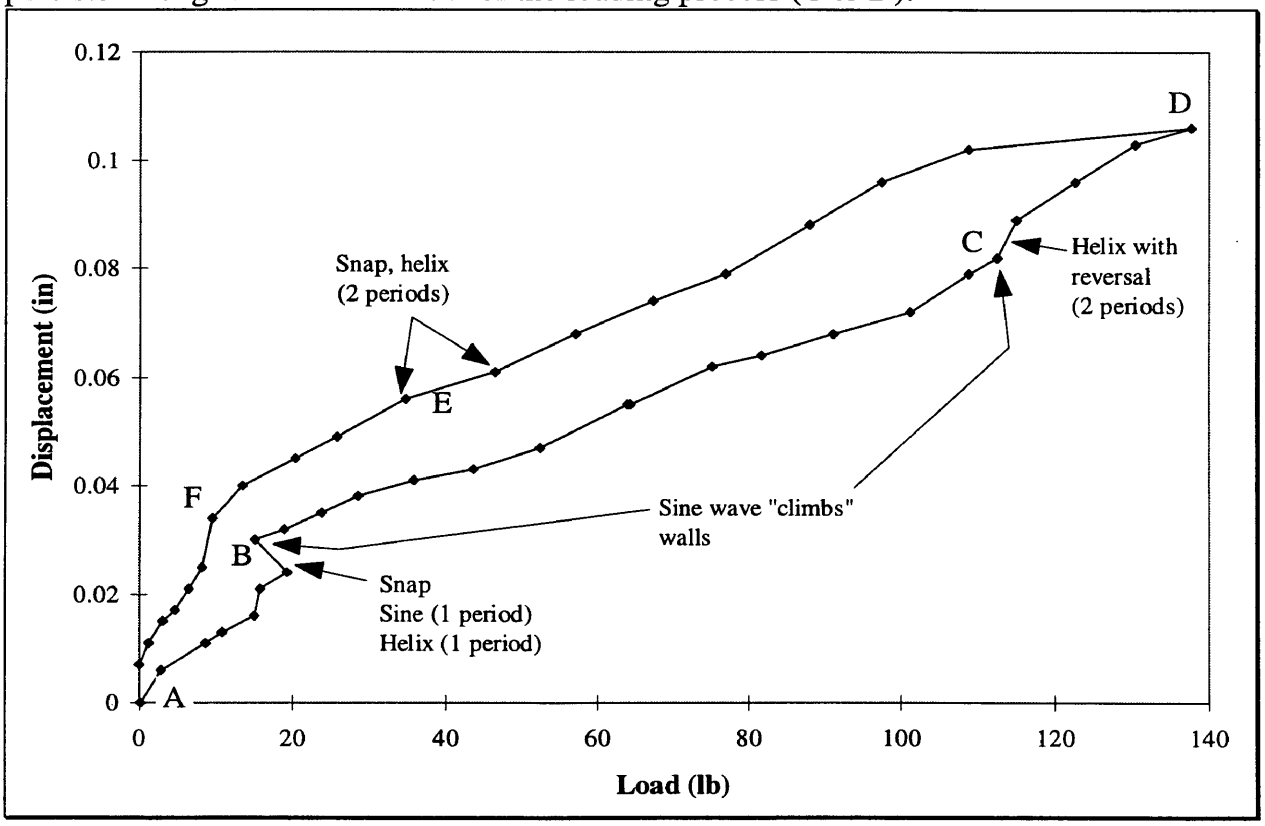

Figure 2. Typical buckling curve for 1/4 in. rod in straight borehole.

During the unloading process (DFA), the pitch of the two helixes lengthens slightly until a snap occurs that removes the helix (point E). At this point, a helix exists with a

pitch of 6 feet (2 periods along the entire length). The helix continues to unwind until a sine wave (1-1/2 or 2 periods) exists along the bottom of the borehole (E to F). Further decrease in the load straightens the rod to its initial state (F to A).

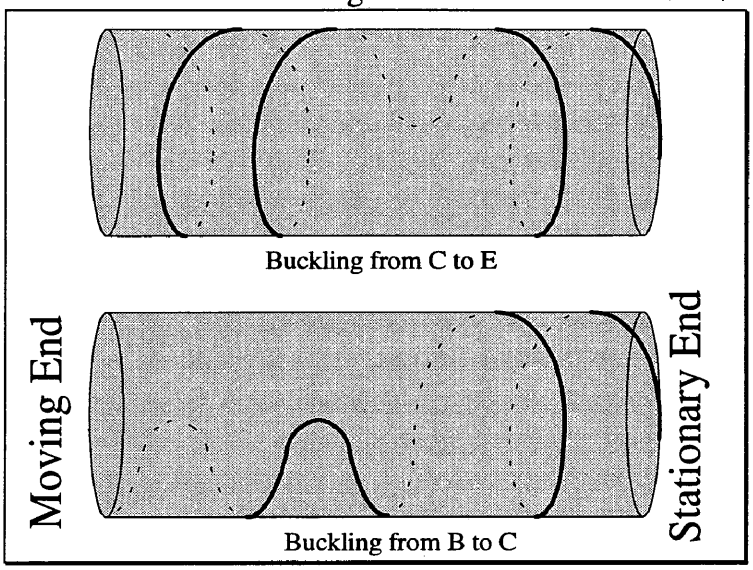

Figure 3. Helix development in straight borehole.

Suryanaryana and McCann determine the critical helical buckling load from the point where the slope change occurs. This particular loading curve has a snap that occurred at the helical buckling load, shown by the sudden drop in load. The unloading curve is much smoother and the helical buckling load is easier to see. Compared with the values calculated in Table 2, the load calculated with Chen's equation agrees with the unloading curve and the method developed by Suryanarayana agrees more closely with the loading curve. At this point, a helix with one period exists at the stationary end and a sine wave with one period exists at the moving end. The entire length of the rod does not buckle helically until much higher loads.

Buckling in a Curved Borehole

Buckling behavior in the curved borehole is dramatically different from that in a straight borehole. Initially, the rod is on the bottom of the borehole but when buckling first occurs the ends of the rod rise to the top of the borehole (see Figure 4). The rod remains in contact with the bottom of the hole at the high spot. As the load increases the rod begins to buckle sinusoidally in a horizontal plane. Near the high spot of the borehole, the rod transitions from the top of the borehole to the bottom and back to the

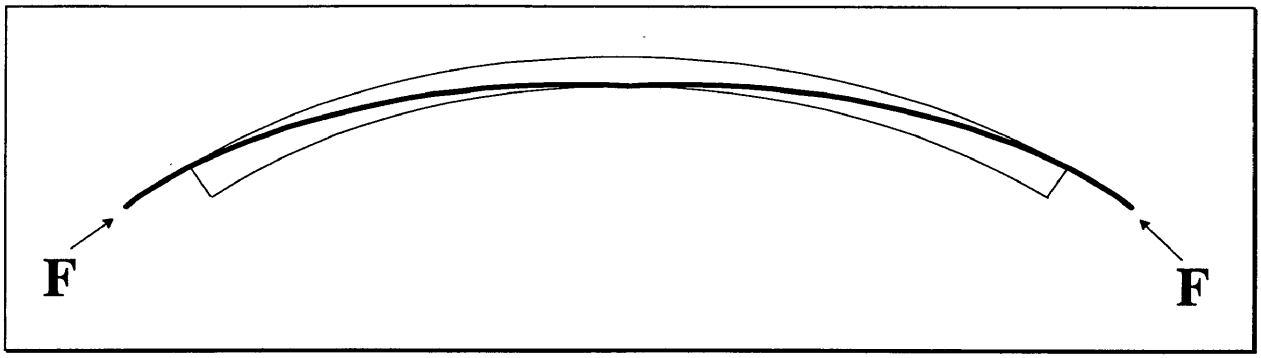

Figure 4. Initial buckling configuration in curved borehole.

top again. In this transition region, the rod will remain in contact with the side of the borehole but oftentimes it was observed that the rod actually leaves the wall of the borehole for short distances. This was especially pronounced during the unloading process when the rod would not contact the wall for significant distances.

Helix development begins at the ends of the borehole, away from the high spot. A long helix would develop at both ends with either a helix reversal in the center, or a short section of sinusoidally buckled rod. When the load was further increased, a very loud, audible snap would occur which transforms the rod into a helix with 3 to 4 periods. Upon unloading, the helix would slowly unwrap itself until a sine wave formed along the top of the borehole. At the high spot, the sinusoid would then "walk" around to the bottom of the borehole, while the rod away from the center remained on the top. As the rod was unloaded further, the transition region from top to bottom would not touch the wall of the borehole for distances of up to one foot.

A typical buckling cycle for a curved borehole is shown in Figure 5. The beginning of the process shows where the rod does not touch the side of the borehole for short distances at both ends. As the load increases, the rod is forced to the top of the borehole and a sine wave develops (B to C). These sine waves usually transition from the top of the borehole to the bottom or side of the borehole near the high spot. With further increase in the load, a very loud snap occurs and the load is reduced dramatically (C to D). At this point, the first helix has developed at the stationary end with a sine wave at the moving end. As the load increases (D to E) another snap occurs and the rod becomes helically buckled along its entire length (E to F). With increasing load snapping continues and the number of periods increase; the helix becomes "tighter."

Upon unloading (GHJA), the helix unwinds itself to the point where a sinusoid exists at the moving end and a helix exists at the stationary end (H to J). Eventually, the rod becomes sinusoidally buckled along the top of the borehole, then segments at both ends move away from the wall of the borehole again, until finally the rod settles back down to the bottom of the borehole (J to A).

The critical load, where the change in slope occurs (point B), is much lower than in the straight borehole, but the displacement is higher. It is likely that the higher displacement occurs because the rod is not constrained by the wall of the borehole at this point, and it is free to buckle or bend in any direction.

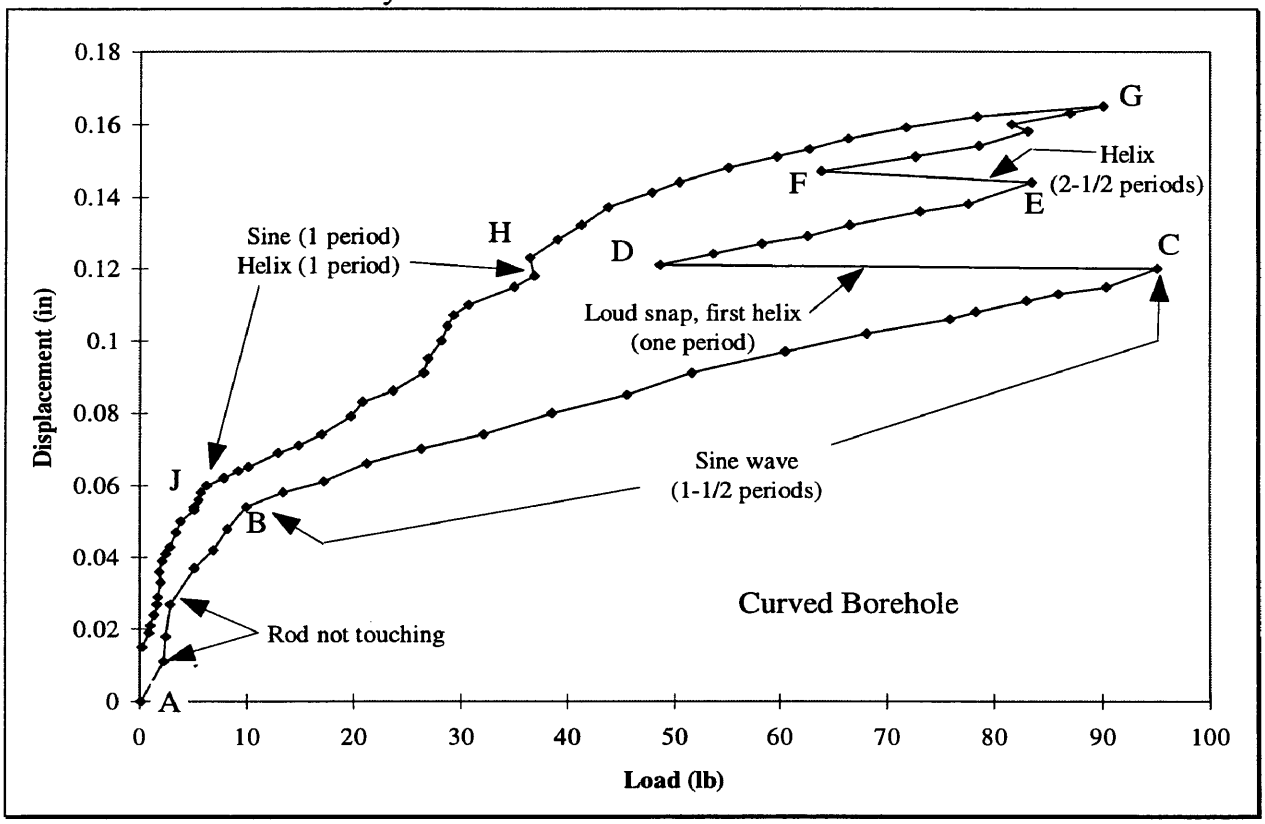

Figure 5. Typical buckling curve for 1/4 in. rod in 65°/100 ft dogleg.

Straight-Curved Borehole Comparison

In Figure 6 curves are shown for the buckling process in a straight borehole and two different dogleg severities, 33°/100 ft and 65°/100 ft. The shapes of the buckling curves for the two doglegs are very similar but differ in magnitude. For increased dogleg severity the initial buckling process has higher displacements with the change in slope occurring at lower loads. The higher dogleg also snaps into the tight helix at much lower loads than does the more straight boreholes.

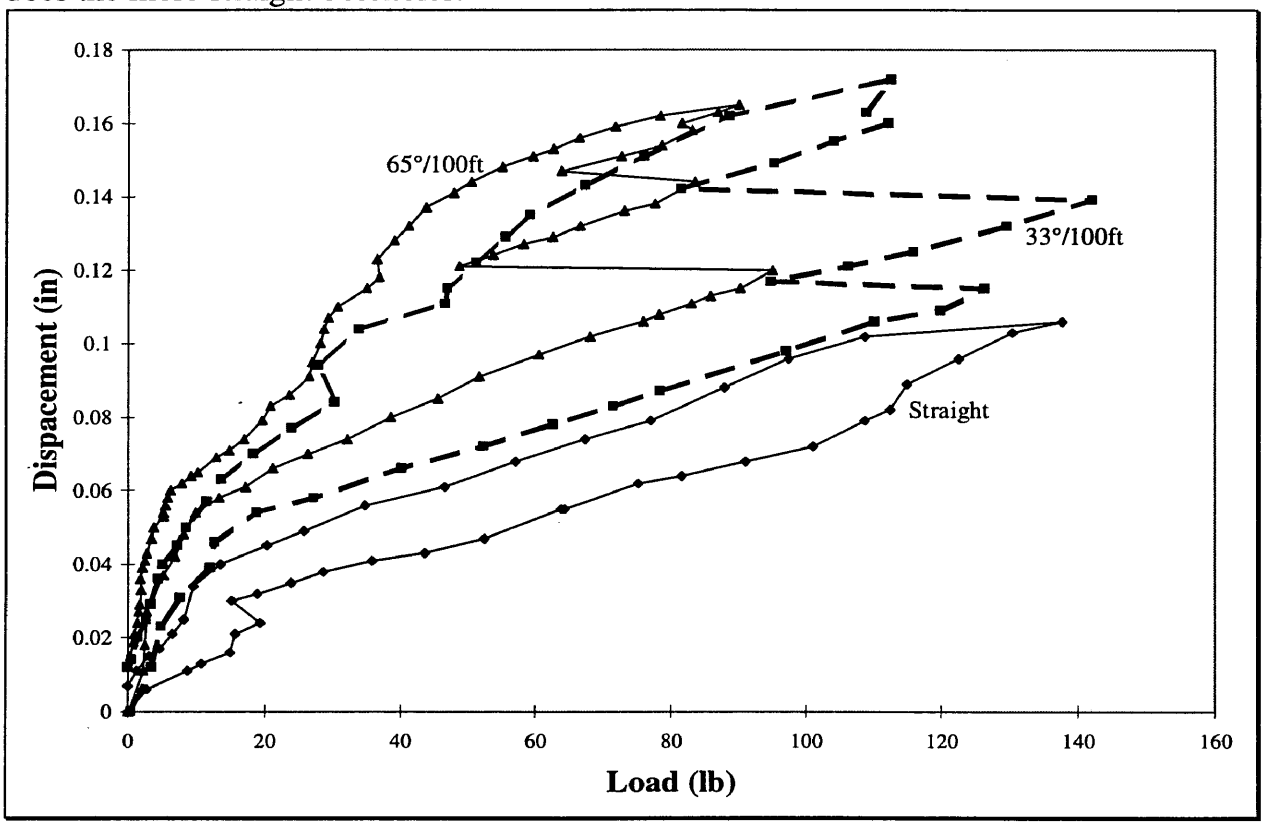

Figure 6. Effect of dogleg severity on the buckling behavior.

A similar plot is shown in Figure 7, but only the loading portion is shown. This clearly shows the difference in the point where the slope change occurs for each curve. The values calculated in Table 2 do not agree with this point for the higher doglegs. In the derivation of the equations used to calculate the values in Table 2, the assumption is made that the rod is in a helix that remains in contact with the wall of the wellbore. For the

curved wellbore, this assumption may not be valid since the rod actually leaves the wall of the wellbore in some segments.

Current theory suggests that once the critical helical buckling load is reached, the rod is helically buckled along its entire length. Suryanarayana suggested that since these theories were developed for the friction-less case they actually predict the minimum energy required to sustain the rod in a helix. The laboratory experiments performed for this paper indicate that this is indeed the case. The rod is not helically buckled, by visual observations, at the critical load as found by the change in slope on the loading curve. However, upon unloading the rod maintains this helical shape until the change in slope occurs.

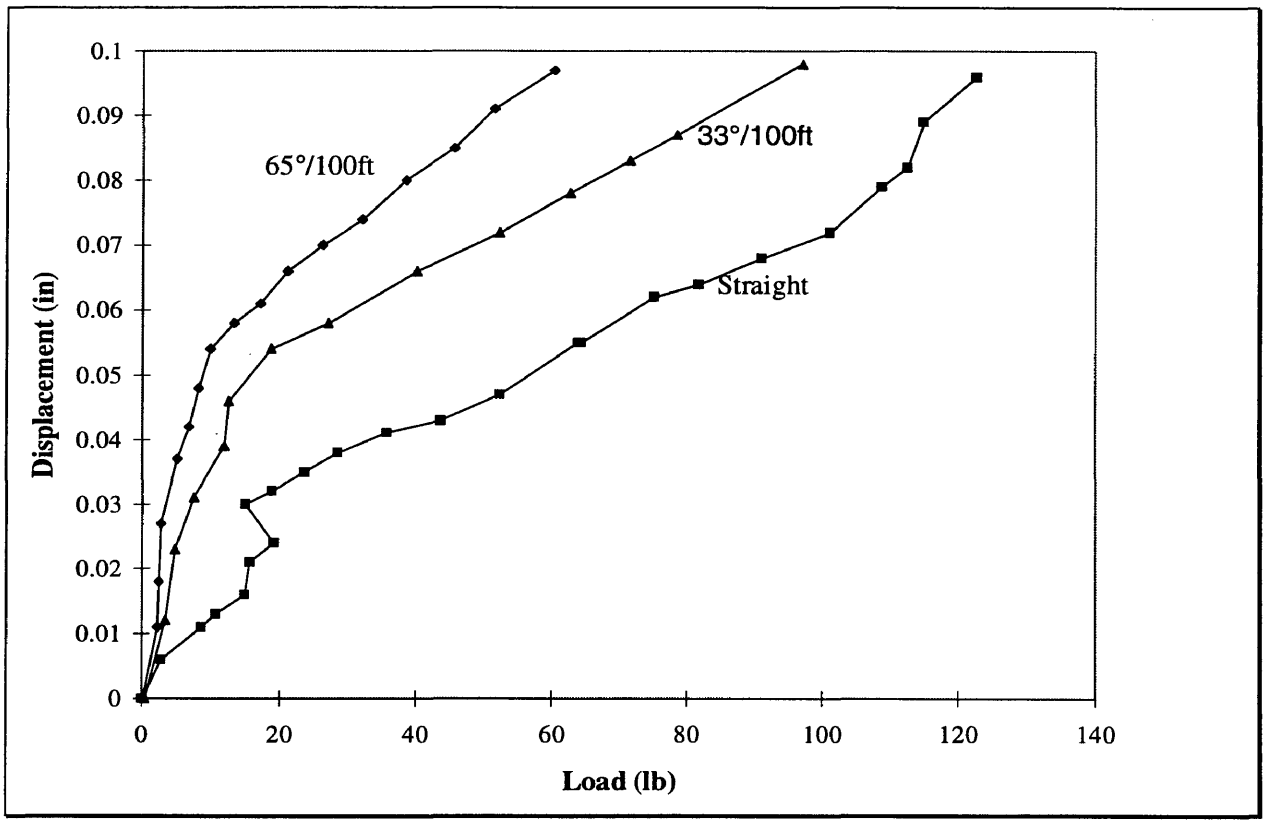

Figure 7. Effect of dogleg severity on initial buckling behavior.

Visual observations in the curved borehole show that there is not a distinct transformation from sinusoidal buckling to helical buckling but rather a transition between the two regions. The helical buckling load taken at the point where the slope change

occurs is near the value predicted by theory (especially for the unloading curve), but a helix does not exist at this point. It is important to note that the first helix does not form until the first snap occurs at C-D in Figure 5.

In the straight borehole, the normal force the rod puts on the wall of the borehole is seen in the initial buckling process, see Figure 7, just before the change in slope occurs. As the axial load increases, the normal forces also increase, thereby increasing the friction, and higher loads are required for a given displacement. In the curved borehole the rod does not contact the wall in some places, which results in lower normal forces and lower friction. Since the rod does not contact the borehole along its entire length the friction is not uniformly distributed along the entire length. The result is that lower axial loads are required for a given displacement. As the wellbore curvature increases the rod experiences even more freedom to preferentially buckle, resulting in less friction and lower loads.

As the buckling proceeds up the load curve, the straight borehole configuration results in larger and larger normal forces and resultant friction. In order for any helix reversals to be removed the energy in the system must become significant enough to overcome the frictional forces and "drive" the reversal out by sliding the rod along the wall. This does not guarantee that the reversal will be removed completely but simply moved to accommodate a lower energy state that is balanced by the frictional forces. This would explain why, in the straight borehole, the reversals were not completely removed until unloading occurred and the frictional forces were lower.

In the curved borehole configuration, the friction is lower and the snapping occurs at much lower loads. The sine waves do not have to climb the wall, overcoming friction, as in the straight borehole. The curvature of the borehole provides for a less constrained sinusoidal development that will transition into a helix at much lower loads. Because of the lower friction, less energy is required to snap the helix reversals out of the system, which are always removed completely while loading rather than unloading.

Repeatability

Figure 8 shows the repeatability of three different data sets taken for a straight borehole (Data for curved boreholes is shown in Appendix D). At a load of 5.0 lbs the displacement varies from 0.0058 in. to 0.0145 in.

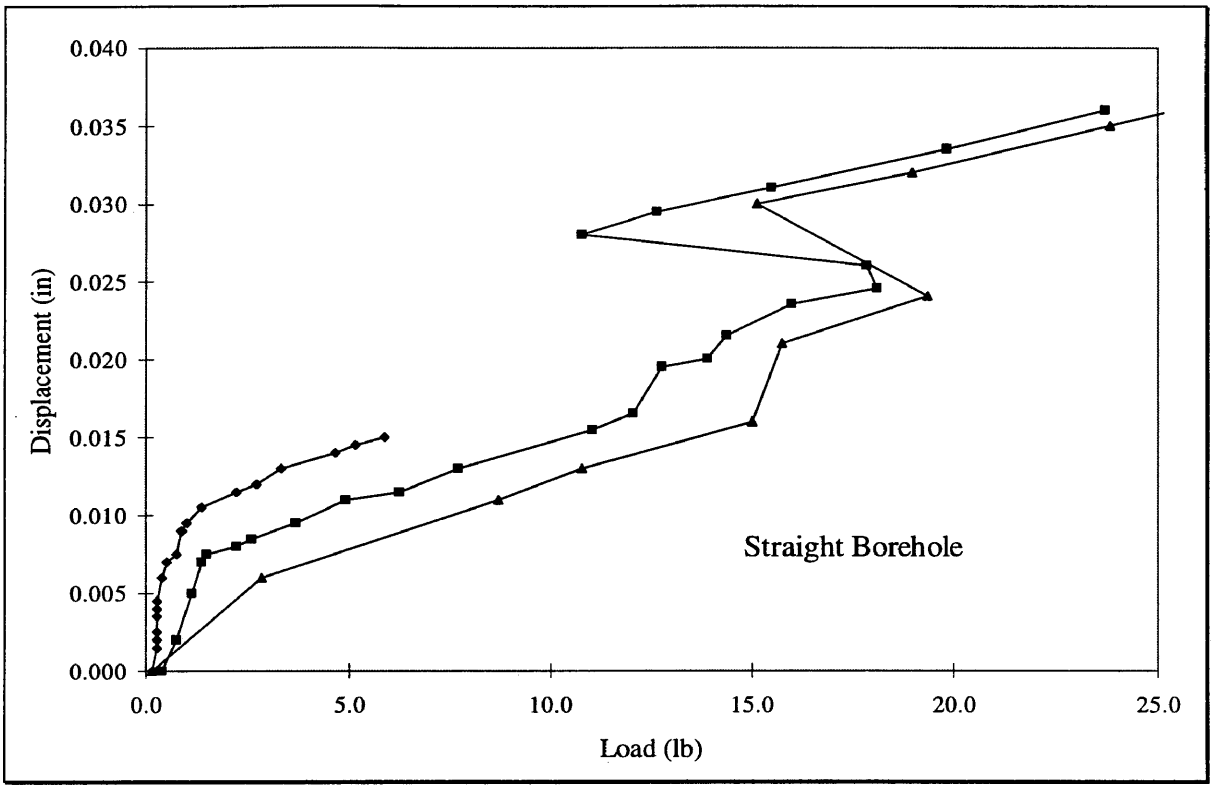

Figure 8. Repeatability of data from straight borehole (loading only)

Loading at Stationary End

Figure 9 shows a comparison of the loading at the stationary end as compared to the loading at the moving end (data for curved boreholes is shown in Appendix D). The vertical axis is the displacement at the moving end. At a displacement of 0.060 in. the load is 125 lbs for the stationary end and 73 lbs for the moving end on the loading portion of the curve. On the unloading portion of the curve the load is 100 lbs for the stationary end and 45 lbs for the moving end. The loading difference between the two ends is 52 lbs and 55 lbs for the loading and unloading curves, respectively, with the stationary end being larger in all cases.

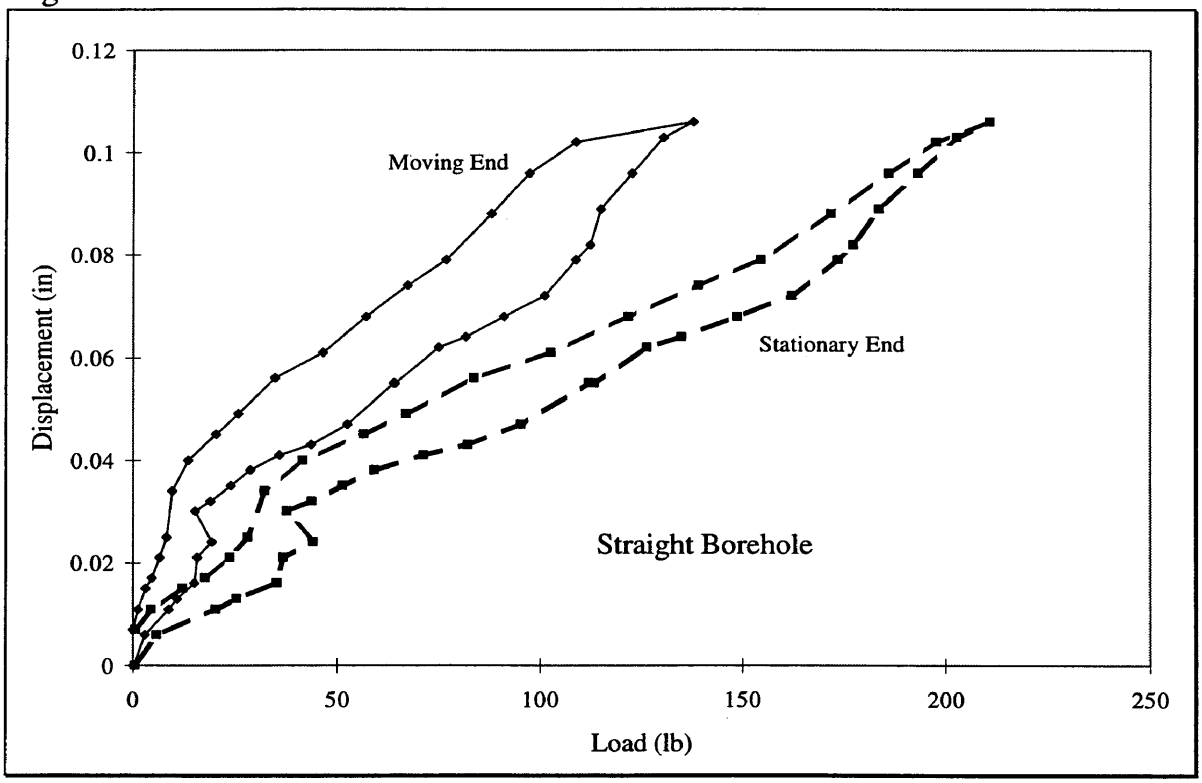

Figure 9. Stationary load/moving load comparison for straight borehole.

FUTURE WORK

The buckling behavior observed in this paper is obviously affected by friction between the rod and the wall of the borehole. The significance of this effect is to be the subject of future work. The following behaviors are possibly the result of frictional effects: 1.) formation of the first helix at the stationary end rather than at the moving end; 2.) helix reversals and the snapping behavior that removes them; 3.) lower loads and higher displacements for increased borehole curvature; 4.) non-constant pitch along the length of the buckled rod for curved boreholes, and; 5.) formation of the first helix at a significantly higher load for curved boreholes. It is recommended that studies be made using a vibrating apparatus attached to the borehole in order to minimize the friction. This should more accurately depict actual oil field operations. The relationship between the loads at the stationary and moving ends should also be analyzed to determine how much of the loading force is being transmitted into normal forces along the walls.

CONCLUSIONS

An experimental laboratory apparatus was built to simulate the buckling of a drillpipe in a curved borehole. Experiments were run to simulate buckling and unbuckling in varying degrees of dogleg severity. Results verify that current theories predicting critical buckling loads actually predict the unbuckling load in a straight borehole. During loading it was observed that the expected critical helical buckling load does not always coincide with a fully developed helix along the entire length of the rod. The buckling process never transitions directly from sinusoidal to helical without some degree of both types existing at the same time. The sine waves always climb the walls until several helixes exist, with reversals that require some degree of snapping to remove. In the straight borehole the reversals are not removed until unloading occurs when the frictional forces are lowered.

With increasing borehole curvature, the buckling loads are reduced below that predicted by current theories. Observations indicate that with borehole curvature the rod is not always in contact with the wall of the wellbore as theories assume. This results in lower normal forces between the rod and the wall of the wellbore, decreasing the frictional effects and lowering the buckling loads. Helix reversals are removed at much lower loads than in a straight borehole so that the rod assumes a helical shape sooner. These results indicate that in a borehole with any curvature at all, a tubular would buckle helically, ultimately resulting in lock-up, much sooner than current theories predict.

REFERENCES

1. Shigley, Joseph Edward, and Mischke, Charles R., 1989. Mechanical Engineering Design-5th Edition. New York; McGraw-Hill.

2. Pasley, P.R., and Bogy, D. B., 1964. "The Stability of a Circular Rod Laterally Constrained to be in Contact With an Inclined Circular Cylinder." ASME Journal Applied Mechanics, Vol. 31; pp. 605-610.

3. Dawson, R., and Paslay, P.R., 1984. "Drillpipe Buckling in Inclined Holes." Journal of Petroleum Technology, October 1984, pp 1734-1738.

4. Suryanarayana, P.V.R., and McCann, R. C., 1994. "Experimental Study of Buckling and Post-Buckling of Laterally Constrained Rods: Part 1 - Frictional Effects." The American Society of Mechanical Engineers.

5. Lubinski, A., Althouse, W.S., and Logan, J. L., 1962. "Helical Buckling of Tubing Sealed in Packers." Journal of Petroleum Technology, June 1962, pp 655-670.

6. Chin, Y., Lin, Y., and Cheatham, J. B., 1990. "Tubing and Casing Buckling in Horizontal Wells." Journal of Petroleum Technology, February 1990, pp 140-191.

APPENDIX A: DERIVATIONS

Euler Buckling Load

Assume a bar of length l loaded by a force F acting along the centroidal axis on rounded or pinned ends (see Figure A1). The bar is bent in the positive y direction which requires a negative moment, hence

$$M = -Fy \tag{A1}$$

From the flexure of beams we know

$$\frac{\partial^2 y}{\partial x^2} = \frac{M}{EI} = -\frac{F}{EI} y \tag{A2}$$

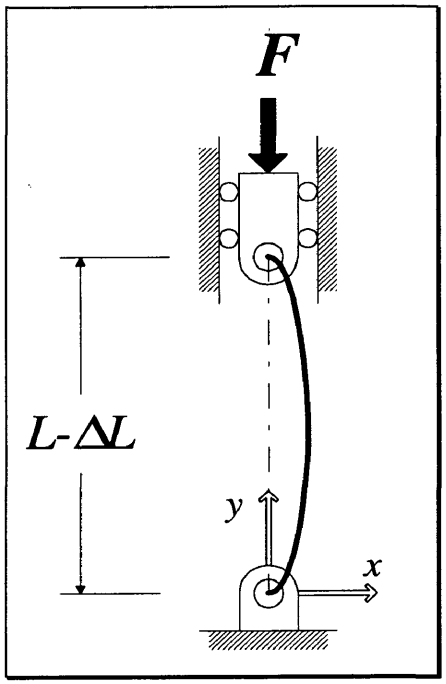

Figure A1. Euler Buckling.

or

$$\frac{\partial^2 y}{\partial x^2} + \frac{F}{EI} y = 0 \tag{A3}$$

This is a differential equation for simple harmonic motion with the solution

$$y = A \sin \sqrt{\frac{F}{EI}} x + B \cos \sqrt{\frac{F}{EI}} x \tag{A4}$$

where A and B are constants of integration that are determined from the boundary conditions $y = 0$ at $x = 0$ and at $x = L$. This gives $B = 0$ and

$$0 = A \sin \sqrt{\frac{F}{EI}} L \tag{A5}$$

The trivial solution of no buckling occurs when $A = 0$. When $A \neq 0$ then

$$\sin\sqrt{\frac{F}{EI}}L=0 \tag{A6}$$

This equation is satisfied when

$$\sqrt{\frac{F}{EI}}L=n\pi \quad n = 1, 2, 3, \ldots \tag{A7}$$

Solving for F when $n = L$ gives the first critical load which is called the *Euler column formula*

$$F_{cr}=\frac{\pi^2 EI}{L^2} \tag{A8}$$

This equation applies only to columns with ends pinned as in the figure. Critical loads for columns with different end conditions can be obtained by solving the differential equation with the appropriate boundary conditions. For the purposes of this paper, only the bar with pinned ends is considered.

Using the relation $I=Ak^2$, where A is the cross-sectional area and k is the radius of gyration, allows the more convenient form to be written

$$\frac{F_{cr}}{A}=\frac{\pi^2 E}{(L/k)^2} \tag{A9}$$

Paslay and Bogy: Critical Buckling Load (Sinusoidal)

Paslay and Bogy used energy methods to examine the stability of a rod in an inclined cylinder. Restrictions were placed on the displacement such that the rod is always in contact with the wall of the cylinder and the rod does not rotate as it moves around the cylinder.

The initial configuration and loading are shown in Figure A2. Loading is the result of the

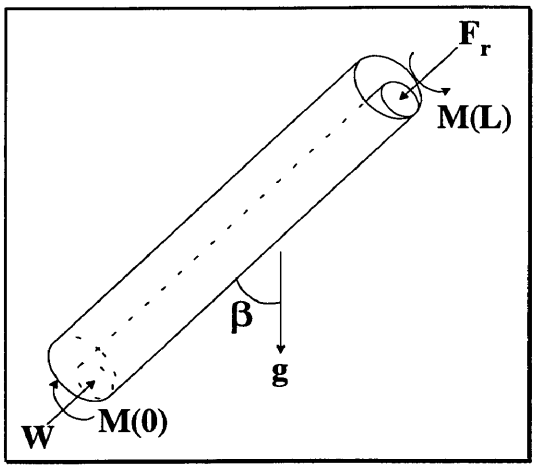

Figure A2

gravitational field applied at an angle β and the axial load, F_r, applied at the upper end of the rod.

The stability criteria are obtained by minimizing the total potential energy, U, of the system. The total potential energy of the system is given by

$$U = U_s + U_f \tag{A10}$$

The change in the potential energy from the initial equilibrium position is given by

$$\Delta U = \delta U_s + \delta U_f + \frac{1}{2!}\delta^2 U_s + \frac{1}{2!}\delta^2 U_f + \frac{1}{3!}\delta^3 U_s + \frac{1}{3!}\delta^3 U_f + \ldots \tag{A11}$$

where $\delta^n U_s$ and $\delta^n U_f$ contain the n-th order terms.

The conditions for stable equilibrium are

$$\begin{aligned} \partial U_s + \partial U_f &= 0 \\ \partial^2 U_s + \partial^2 U_f &> 0 \end{aligned} \tag{A12}$$

A cross section of the initial configuration is shown in figure A3. The position of a particle P_o can be described with the cylindrical coordinate system (r, α, z). The initial configuration can be written

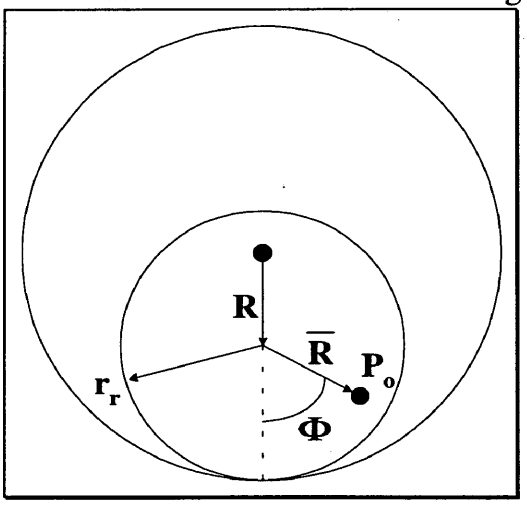

Figure A3

$$\begin{aligned} r_i &= \sqrt{\left(R + \bar{R}\cos\Phi\right)^2 + \left(\bar{R}\sin\Phi\right)^2} \\ \alpha_i &= \tan^{-1}\left(\frac{\bar{R}\sin\Phi}{R + \bar{R}\cos\Phi}\right) \\ z_i &= Z \end{aligned} \tag{A13}$$

In order to obtain the strains we need to obtain the difference in lengths of line elements between the unstressed and stressed line elements. Since the diameter of the rod is constant and it remains in

contact with the wall of the cylinder, both R and r remain constant. Two adjacent particles, P_0 and P, are given by

$$P_o(\overline{R},\Phi,Z) \qquad P(\overline{R}+d\overline{R},\Phi+d\Phi,Z+dZ) \tag{A14}$$

and the distance between them can be written as

$$(dS)^2=(d\overline{R})^2+(\overline{R}d\Phi)^2+(dZ)^2 \tag{A15}$$

After displacement, the coordinates of P_o change, as shown in figure A4. The assumption is made that the coordinates can be described by four parameters: ε_1, ε_2, Φ, and ξ, where ε_1 and ε_2 are constants, and Φ and ξ are functions of Z. Therefore, after displacement the coordinates of P_o are

$$\begin{aligned} r&=\sqrt{[R+\overline{R}\cos(\Phi+\phi)]^2+[\overline{R}\sin(\Phi+\phi)]^2} \\ \alpha&=\xi+\tan^{-1}\left(\frac{\overline{R}\sin(\Phi+\phi)}{R+\overline{R}\cos(\Phi+\phi)}\right) \\ z&=\left(1+\varepsilon_1+\frac{\varepsilon_2}{2L}Z\right)Z-R\overline{R}\xi'\sin(\Phi+\phi) \end{aligned} \tag{A16}$$

where ξ' denotes differentiation with respect to Z.

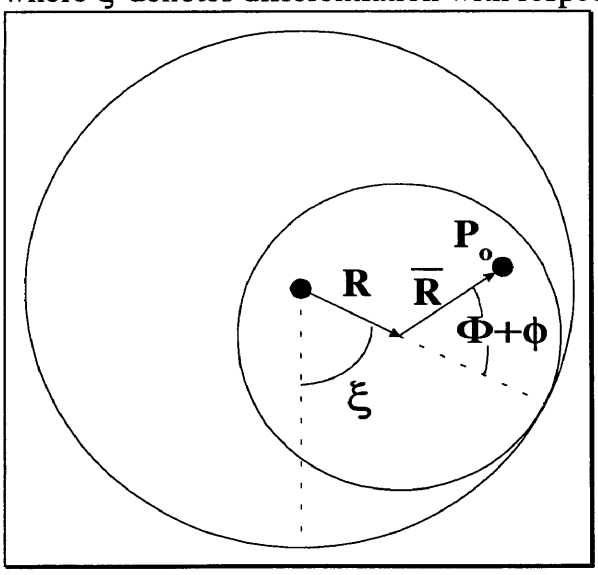

Figure A4

Paslay and Bogy noted that no precise physical significance can be given to the parameters ε_1, ε_2, Φ, and ξ but there is a useful interpretation. The uniform strain of the rod due to the axial loading, F_r, corresponds to ε_1. The varying strain of the rod due to its own weight corresponds to ε_2. The moment *M(L)* induces an angle of twist that corresponds to ϕ and the lateral displacement of the rod from the low side of the hole corresponds to $R\xi$. The parameters ε_1 and ε_2 enter only into the axial motion of the rod. For sufficiently small loading, the

parameter ξ is equal to zero but when the loading grows to the point where an instability occurs, ξ is not equal to zero.

The distance between the two points P_o and P are now given by

$$
\begin{aligned}
(ds)^2 &= (d\overline{R})^2\left[1+R^2(\xi')^2\sin^2(\Phi+\phi)\right]+(d\Phi)^2\left[\overline{R}^2+R^2\overline{R}^2(\xi')^2\cos^2(\Phi+\phi)\right] \\
&+(dZ)^2\left\{\begin{array}{l}\overline{R}^2(\phi')^2\left[1+\overline{R}^2(\xi')^2\cos^2(\Phi+\phi)\right]+(\xi')^2\left[R^2+2R\overline{R}\cos(\Phi+\phi)\right] \\ +\left[2\overline{R}\left(R\cos(\Phi+\phi)+\overline{R}\right)-2R\overline{R}\left(1+\varepsilon_o\right)\cos(\Phi+\phi)\right]\xi\phi'+\left(1+\varepsilon_o\right)^2 \\ -2\left(1+\varepsilon_o\right)R\overline{R}\xi''\sin(\Phi+\phi)+R^2\overline{R}^2(\xi'')^2\sin^2(\Phi+\phi) \\ +2R^2\overline{R}^2\xi''\xi\phi'\cos(\Phi+\phi)\sin(\Phi+\phi)\end{array}\right\} \\
&+2d\overline{R}d\Phi\left[R^2\overline{R}(\xi')^2\cos(\Phi+\phi)\sin(\Phi+\phi)\right] \\
&+2d\Phi dZ\left\{\overline{R}^2\phi'+\overline{R}^2\xi'+R\overline{R}\xi'\cos(\Phi+\phi)\left[-\varepsilon+R\overline{R}\left(\xi''\sin(\Phi+\phi)+\xi\phi'\cos(\Phi+\phi)\right)\right]\right. \\
&+2dZd\overline{R}\left.\left\{\overline{R}\xi'\sin(\Phi+\phi)\left[-\varepsilon+R\overline{R}\left(\xi''\sin(\Phi+\phi)+\xi\phi'\cos(\Phi+\phi)\right)\right]\right\}\right.
\end{aligned}
\tag{A17}
$$

where

$$\varepsilon_o = \varepsilon_1 + \frac{\varepsilon_2 Z}{L} \tag{A18}$$

If the following parameters are defined as

$$
\begin{aligned}
E_{\overline{R}\overline{R}} &= \frac{1}{2}R^2(\xi')^2\sin^2(\Phi+\phi) \\
E_{\Phi\Phi} &= \frac{1}{2}R^2\overline{R}^2(\xi')^2\cos^2(\Phi+\phi) \\
E_{ZZ} &= \varepsilon_o - R\overline{R}\xi''\sin(\Phi+\phi)+\frac{1}{2}\overline{R}^2(\phi')^2+\frac{1}{2}(\xi')^2\left[R^2+2R\overline{R}\cos(\Phi+\phi)+\overline{R}^2\right] \\
&+\overline{R}^2\xi\phi'+\frac{1}{2}\varepsilon_o{}^2-R\overline{R}\varepsilon_o\xi''\sin(\Phi+\phi)+\frac{1}{2}R^2\overline{R}^2(\xi'')^2\sin^2(\Phi+\phi) \\
&-R\overline{R}\varepsilon_o\xi\phi'\cos(\Phi+\phi)+R^2\overline{R}^2(\xi')^2\xi''\phi'\cos(\Phi+\phi)\sin(\Phi+\phi) \\
&+\frac{1}{2}R^2\overline{R}^2(\phi')^2(\xi')^2\cos^2(\Phi+\phi)
\end{aligned}
\tag{A19}
$$

$$2E_{\bar{R}\Phi} = R^2\bar{R}(\xi')^2\cos(\Phi+\phi)\sin(\Phi+\phi)$$
$$2E_{\Phi Z} = \bar{R}^2\xi' + \bar{R}^2\phi' - R\bar{R}\xi\varepsilon_o\cos(\Phi+\phi) + R^2\bar{R}\xi\xi''\cos(\Phi+\phi)\sin(\Phi+\phi)$$
$$+R^2\bar{R}^2(\xi')^2\phi'\cos^2(\Phi+\phi)$$
$$2E_{Z\bar{R}} = -R\xi\varepsilon_o\sin(\Phi+\phi) + R^2\bar{R}\xi\xi''\sin^2(\Phi+\phi)$$
$$+R^2\bar{R}(\xi')^2\phi'\cos(\Phi+\phi)\sin(\Phi+\phi)$$

then equation (A20) minus equation (A21) yields

$$(ds)^2 - (dS)^2 = 2E_{\bar{R}\bar{R}}(d\bar{R})^2 + 2E_{\Phi\Phi}(d\Phi)^2 + 2E_{ZZ}(dZ)^2 + 4E_{R\Phi}d\bar{R}d\Phi \quad \text{(A22)}$$
$$+4E_{\bar{R}Z}d\bar{R}dZ + 4E_{\Phi Z}d\Phi dZ$$

which is the difference in the length of the un-strained and strained elements.

The strain energy can now be written

$$U_s = \int_{\bar{R}=0}^{r}\int_{\Phi=0}^{2\pi}\int_{Z=0}^{L}\left[\begin{array}{l}\dfrac{G\nu}{1-2\nu}\left(E_{\bar{R}\bar{R}} + \dfrac{1}{\bar{R}^2}E_{\Phi\Phi} + E_{ZZ}\right)^2 \\ +G\left(E_{\bar{R}\bar{R}}E_{\bar{R}\bar{R}} + \dfrac{1}{\bar{R}^2}E_{\Phi\Phi}\dfrac{1}{\bar{R}^2}E_{\Phi\Phi} + E_{ZZ}E_{ZZ}\right. \\ \left. + \dfrac{2}{\bar{R}^2}E_{\Phi\bar{R}}E_{\Phi\bar{R}} + \dfrac{2}{\bar{R}^2}E_{\Phi Z}E_{\Phi Z} + 2E_{\bar{R}Z}E_{\bar{R}Z}\right)\end{array}\right]\bar{R}d\bar{R}d\Phi dZ \quad \text{(A23)}$$

and the potential energy of the axial force, F_r, is

$$U_f = F_r\left(1+\varepsilon_1+\frac{\varepsilon_2}{2}\right)L - M\xi(L) - M\phi(L) \quad \text{(A24)}$$
$$+\int_0^L \rho Ag\left[\left(1+\varepsilon_1+\varepsilon_2\frac{Z}{2L}\right)Z\cos\beta + (1-\cos\xi)R\sin\beta\right]dZ$$

If equations (A19) are substituted into equation (A23), the integration is carried out on $\bar{R}$ and Φ, the results along with equation (A24) are substituted into equation (A10) and a very lengthy expression can be written for U. This expression can be simplified if it is assumed that ε_1, ε_2, ϕ, and ξ are much smaller than 1 and are replaced with $\varepsilon_{1_0}+\delta\varepsilon_1$, $\varepsilon_{2_0}+\delta\varepsilon_2$, $\phi_o+\delta\phi$, and $\xi_0+\delta\xi$ then the potential energy can be written as

$$U \rightarrow U + \Delta U = U + \delta U + \frac{1}{2!}\delta^2 U + \ldots \quad \text{(A25)}$$

The condition imposed by equations (A12) leads to the equilibrium solution

$$\varepsilon_{1_0} = -\frac{\rho AgL\cos\beta}{\pi r_r^{\,2}\overline{E}} - \frac{F_r}{\pi r_r^{\,2}\overline{E}}$$
$$\varepsilon_{2_0} = \frac{\rho AgL\cos\beta}{\pi r_r^{\,2}\overline{E}} \tag{A26}$$
$$\xi_0 = 0$$
$$\phi = \frac{2ML}{G\pi r_r^{\,4}}\frac{Z}{L}$$

where

$$\overline{E} = \frac{2G(1-\nu)}{(1-2\nu)} \tag{A27}$$

Using the condition ε_{1_0}, ε_{2_0},and ϕ are much less than 1 the second order terms in equation(A25) are

$$\frac{1}{2}\delta^2 U = \frac{1}{2}\pi\overline{E}r_r^{\,2}\int_0^L\left(\delta\varepsilon_1 + \frac{Z}{L}\delta\varepsilon_2\right)^2 dZ + \frac{1}{4}\pi G r_r^{\,4}\int_0^L(\delta\phi' + \delta\xi')^2 dZ$$
$$+\frac{1}{8}\pi\overline{E}R^2 r_r^{\,4}\int_0^L(\delta\xi'')^2 dZ + \frac{1}{2}\rho AgR\sin\beta\int_0^L(\delta\xi)^2 dZ \tag{A28}$$

This equation is positive definite for all possible variations about the equilibrium solution. The only instabilities occur when the second integral vanishes by the restriction

$$\delta\phi' = -\delta\xi' \tag{A29}$$

This leads to

$$\frac{1}{2}\delta^2 U = \frac{1}{2}\pi\overline{E}r_r^{\,2}\int_0^L\left(\delta\varepsilon_1 + \frac{Z}{L}\delta\varepsilon_2\right)^2 dZ - \frac{\pi GR^2 r_r^{\,2}}{1-2\nu}\int_0^L\left(\frac{F}{\pi r_r^{\,2}\overline{E}} + \frac{\rho AgL\cos\beta}{\pi r_r^{\,2}\overline{E}} - \frac{\rho AgZ\cos\beta}{\pi r_r^{\,2}\overline{E}}\right)(d\xi')^2 dZ$$
$$+\frac{1}{4}\pi\overline{E}r_r^{\,4}(\phi_0')^2\int_0^L(\delta\xi')^2 dZ + \frac{1}{8}\pi\overline{E}R^2 r_r^{\,4}\int_0^L(\delta\xi'')^2 dZ + \frac{1}{2}\rho AgR\sin\beta\int_0^L(\delta\xi)^2 dZ \tag{A30}$$

The variation that leads to the smallest critical load occurs when

$$\delta\varepsilon_1 + \frac{Z}{L}\delta\varepsilon_2 = 0 \tag{A31}$$

The boundary conditions are

$$\delta\xi(0) = \delta\xi(L) = \delta\xi''(0) = \delta\xi''(L) = 0 \tag{A32}$$

If torsion is neglected and the conditions imposed by equations (A31) and (A32) on equation (A30) after integration, there results

$$(1-\nu)\delta^2 U = \int_0^L \begin{bmatrix} (1-\nu)\bar{E}IR^2\delta\xi'''' + FR^2\delta\xi'' + \rho AgR^2\delta\xi''(L-Z)\cos\beta \\ -\rho AgR^2\delta\xi'\cos\beta + (1-\nu)\rho AgR\delta\xi\sin\beta \end{bmatrix} \delta\xi dZ \tag{A33}$$

and the limit of stability is given by

$$\begin{aligned} &(1-\nu)\bar{E}IR^2\delta\xi'''' + F_r R^2\delta\xi'' + \rho AgR^2\delta\xi''(L-Z)\cos\alpha \\ &-\rho AgR^2\delta\xi'\cos\beta + (1-\nu)\rho AgR\delta\xi\sin\beta = 0 \end{aligned} \tag{A34}$$

This is a homogeneous fourth-order ordinary differential equation which leads to an eigenvalue problem with solution

$$\begin{aligned} 2(1-\nu)\delta^2 U = &-F_r\frac{(R\pi)^2}{L}\sum_{n=1}^{k} n^2(\xi_0)^2 \\ &+\sum_{n=1}^{k}\left[(1-\nu)\bar{E}R^2L\left(\frac{\pi n}{L}\right)^4 - \frac{1}{2}\rho AgR^2\pi^2 n^2\cos\beta + (1-\nu)\rho AgRL\sin\beta\right](\xi_{0_n})^2 \end{aligned} \tag{A35}$$

For the horizontal configuration $\beta=90°$ equation (A35) becomes

$$2(1-\nu)\delta^2 U = \sum_{n=1}^{k}\left[(1-\nu)\bar{E}IR^2L\left(\frac{\pi n}{L}\right)^4 - F_r R^2 L\left(\frac{\pi n}{L}\right)^2 + (1-\nu)\rho AgRL\right](\xi_{0_n})^2 \tag{A36}$$

The condition which makes zero is the one that yields the critical loads

$$F_{cr(n)} = (1-\nu)\bar{E}I\frac{\pi^2}{L^2}\left(n^2 + \frac{1}{n^2}\frac{L^4\rho Ag}{\pi^4\bar{E}IR}\right) \tag{A37}$$

Dawson, Paslay: Critical Compressive Load (Sinusoidal Buckling)

The derivation of what Dawson and Paslay called the critical compressive load begins with the critical buckling load derived by Paslay and Bogy

$$F_{cr(n)} = \frac{(1-\nu)^2}{(1+\nu)(1-2\nu)}EI\frac{\pi^2}{L^2}\left(n^2 + \frac{L^4\rho Ag}{n^2\pi^4 EIR}\right) \tag{A38}$$

where the $\overline{E}$ in the denominator has been replaced as discussed in the main body of the paper. Dawson and Paslay added a sinβ factor for inclined holes and assumed that Poisson's ratio is approximately equal to 1/3 so the coefficient above becomes 1.0

$$F_{cr(n)} = EI\frac{\pi^2}{L^2}\left(n^2 + \frac{L^4 \rho Ag \sin\beta}{n^2\pi^4 EIR}\right) \tag{A39}$$

For long pipes the initial buckling occurs at higher orders rather than at the first order, and proceeds to higher orders with increasing load. The value of n that gives the lowest value of $F_{cr(n)}$ is found by treating n as a discreet variable and setting the derivative equal to zero

$$\frac{\partial F_{cr(n)}}{\partial n} = 0 = EI\frac{\pi^2}{L^2}\left(2n - \frac{2L^4 \rho Ag \sin\beta}{n^3\pi^4 EIR}\right) \tag{A40}$$

which gives

$$n^2 = \sqrt{\frac{L^4 \rho Ag \sin\beta}{\pi^4 EIR}} \tag{A41}$$

For purposes of this paper only horizontal holes are considered (β = 90°) and ν is not assumed to be equal to 1/3. Therefore, equation (A41) is used in equation (A38) to give

$$F_{cr} = \frac{(1-\nu)^2}{(1+\nu)(1-2\nu)} 2EI\frac{\pi^2}{L^2}\left(\frac{L^4 \rho Ag}{\pi^4 EIR}\right) \tag{A42}$$

Lubinski: Helical Buckling Force

A rod under compression experiences a length change as described by Hooke's law

$$L_c = L - \Delta L = L - L\varepsilon = L\left(1 - \frac{\sigma}{E}\right) \tag{A43}$$

A fully formed helix is shown in Figure A5. In the upper right the figure shows the development of the helix. In one pitch of the helix the rod traverses the distance $2\pi r$ that is represented by the right triangle. The relationship between the force along the rod axis is related to the force along the helix axis by

$$F_r = F \sin\theta \tag{A44}$$

or

$$\sigma = \frac{F \sin\theta}{A} \tag{A45}$$

Substituting equation (A45) into equation (A43) gives

$$L_c = L\left(1 - \frac{F \sin\theta}{EA}\right) \tag{A46}$$

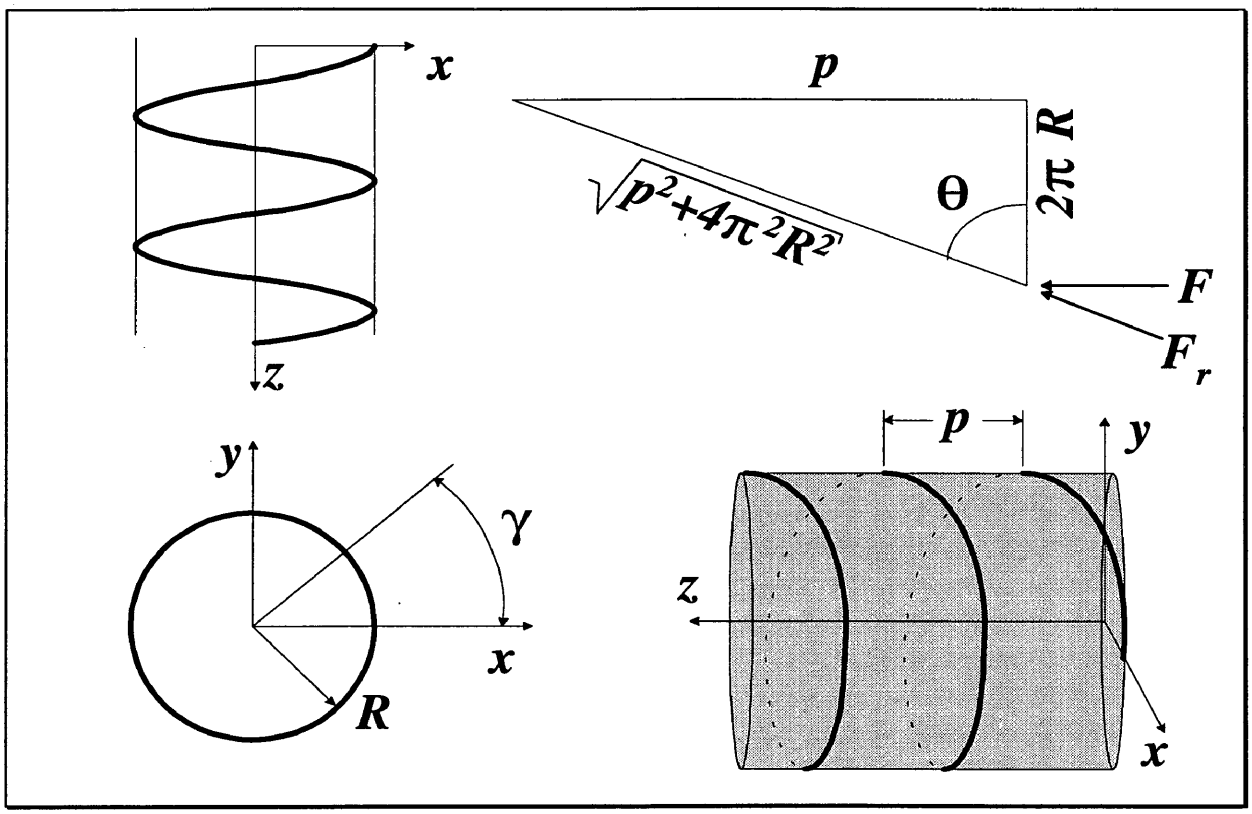

Figure A5. Projections of the helix. Upper right: development of the helix.

The equation for a helix is given in vector form as

$$\mathbf{r}(\theta) = (R\cos\theta)\mathbf{i} + (R\sin\theta)\mathbf{j} + \left(\frac{p}{2\pi}\theta\right)\mathbf{k} \tag{A47}$$

An arbitrary point on the helix is shown by the angle γ, and has x, y, and z coordinates

$$\begin{aligned} x &= R\cos\gamma \\ y &= R\sin\gamma \\ z &= \frac{p}{2\pi}\gamma \end{aligned} \tag{A48}$$

and from calculus the length, s, is given by

$$s = \int_0^{\gamma} \sqrt{\left(\frac{dx}{d\theta}\right)^2 + \left(\frac{dy}{d\theta}\right)^2 + \left(\frac{dz}{d\theta}\right)^2}\, d\theta = \gamma\sqrt{R^2 + \frac{p^2}{4\pi^2}} \tag{A49}$$

Equation (A49) can be solved for the angle γ and substituted into equations (A48) to obtain

$$\begin{aligned} x &= R\cos\left(\frac{2\pi s}{\sqrt{p^2 + 4\pi^2 R^2}}\right) \\ y &= R\sin\left(\frac{2\pi s}{\sqrt{p^2 + 4\pi^2 R^2}}\right) \\ z &= \frac{ps}{\sqrt{p^2 + 4\pi^2 R^2}} \end{aligned} \tag{A50}$$

The strain energy of compression is

$$U_c = \frac{F_r^2 L}{2AE} \tag{A51}$$

Substituting equation (A45) into equation (A51) yields

$$U_c = \frac{F^2 \sin^2\theta L}{2AE} \tag{A52}$$

but from the helix development in figure A5

$$\sin\theta = \frac{p}{\sqrt{p^2 + 4\pi^2 R^2}} \tag{A53}$$

Substituting equation (A53) into equation (A52) yields

$$U_c = \frac{F^2 p^2 L}{2AE\left(p^2 + 4\pi^2 R^2\right)} \tag{A54}$$

The strain energy of bending is given by

$$U_b = \frac{LEIC^2}{2} \tag{A55}$$

The curvature, C, of the vector (A47) is given by the expression

$$C = \sqrt{\left(\frac{d^2x}{ds^2}\right)^2 + \left(\frac{d^2y}{ds^2}\right)^2 + \left(\frac{d^2z}{ds^2}\right)^2} = \frac{4\pi^2 R}{p^2 + 4\pi^2 R^2} \tag{A56}$$

Substituting equation (A56) into equation (A55) the strain energy of bending becomes

$$U_b = \frac{8\pi^4 R^2 EIL}{\left(p^2 + 4\pi^2 R^2\right)^2} \tag{A57}$$

It is assumed that 1) the string is initially straight and remains straight, 2) it stays within the elastic range, and 3) there is no friction between the rod and wall. Therefore, there is no torsion and the strain energy of torsion need not be considered.

The potential energy of the force, F, is

$$U_f = FL_h \tag{A58}$$

From the z component in equation (A50), if z and s are L_h and L_c, respectively, L_h is given by

$$L_h = \frac{L_c p}{\sqrt{p^2 + 4\pi^2 R^2}} \tag{A59}$$

Equations (A46), (A53) and (A59)) can be substituted into equation (A58) to give

$$U_f = \frac{FpL}{\sqrt{p^2 + 4\pi^2 R^2}} - \frac{F^2 p^2 L}{AE\left(p^2 + 4\pi^2 R^2\right)} \tag{A60}$$

The total potential energy of the system is the sum of the compressional strain energy, the bending strain energy, and the potential energy of the force F, given by equations (A54), (A57), and (A60)

$$U = \frac{FpL}{\sqrt{p^2 + 4\pi^2 R^2}} - \frac{F^2 p^2 L}{2AE\left(p^2 + 4\pi^2 R^2\right)} + \frac{8\pi^4 R^2 EIL}{\left(p^2 + 4\pi^2 R^2\right)^2} \tag{A61}$$

Equilibrium occurs when the total potential energy of the system is at a minimum, therefore

$$\frac{dU}{dp}=0 \tag{A62}$$

which leads to

$$\frac{p\left(p^2+4\pi^2R^2\right)}{AE}F^2-\left(p^2+4\pi^2R^2\right)^{3/2}F+8\pi^2EIp=0 \tag{A63}$$

Equation (A63) is a quadratic polynomial in F and the smallest potential energy is obtained from the smallest root

$$F=\frac{AE\sqrt{p^2+4\pi^2R^2}}{2p}\left(1-\sqrt{1-\frac{32\pi^2Ip^2}{A\left(p^2+4\pi^2R^2\right)^2}}\right) \tag{A64}$$

If we assume $p^2 >> 4\pi^2r^2$ then

$$\frac{32\pi^2Ip^2}{A\left(p^2+4\pi^2R^2\right)^2}<<1 \tag{A65}$$

and equation (A64) becomes

$$F=\frac{8\pi^2EI}{p^2} \tag{A66}$$

This equation gives the relationship between the buckling force and the pitch of the helix.

Chen, Lin, and Cheatham: Helical Buckling Load

The bending strain energy and the potential energy of the compressive force are given by

$$U_b=\frac{8\pi^4EILR^2}{p^4}=\frac{8\pi^4EILR^2}{\left(L/n\right)^4} \tag{A67}$$

$$U_f = \frac{2FL\pi^2 R^2}{\left(L/n\right)^2} \tag{A68}$$

When the rod moves into a helix with center of gravity at the center of the hole it undergoes a change in potential energy given by

$$U_p = \rho AgLR \tag{A69}$$

From conservation energy the total energy must be zero

$$U = U_f - U_b - U_p \tag{A70}$$

Substituting the expressions for each energy term and solving for F yields the n-th order helical buckling load

$$F_{hel(n)} = 4EI\frac{\pi^2}{L^2}\left(n^2 + \frac{1}{n^2}\frac{L^4\rho Ag}{8\pi^4 EIR}\right) \tag{A71}$$

The minimizing value of n is found by differentiating with respect to n and setting the result equal to zero, which yields

$$\left(\frac{n\pi}{L}\right)^2 = \sqrt{\frac{\rho Ag}{8EIR}} \tag{A72}$$

Substituting this value of n into equation (A71) gives

$$F_{hel} = 2\sqrt{2}\sqrt{\frac{\rho AgEI}{R}} \tag{A73}$$

Wu, Juvkam-Wold, Lu: Average Helical Buckling Load

Consider the buckling process of the rod in figure A5. The rod is shortened a length ΔL due to the helical buckling

$$\Delta L = L\left(1 - \frac{p}{\sqrt{p^2 + 4\pi^2 R^2}}\right) \approx \frac{2\pi^2 R^2 L}{p^2} \tag{A74}$$

During the buckling process the axial load F does work given by

$$W_f = \int_0^{\Delta L} F dz \tag{A75}$$

As the rod rises off the bottom of the inclined cylinder gravity does negative work on the rod

$$W_g = -\rho A g L R \sin\beta \tag{A76}$$

Wu and Juvkam-Wold state that the work done by gravity along the axis of the helix contributes to the buckling in the same way the force F does but is much smaller and therefore neglected from equation (A76).

The bending energy is given by Lubinski

$$U_b = \frac{8\pi^4 R^2 EIL}{\left(p^2 + 4\pi^2 R^2\right)^2} \approx \frac{8\pi^4 R^2 EIL}{p^4} \tag{A77}$$

and from conservation of energy

$$U_b = W_f + W_g \tag{A78}$$

Substituting equations (A75) thru (A77) into (A78) and rearranging yields

$$\int_0^{\Delta L} F dz = \frac{8\pi^4 R^2 EIL}{p^4} + \rho A g L R \sin\beta \tag{A79}$$

Dividing through by ΔL and noting that $p=L/n$ gives

$$\frac{1}{\Delta L}\int_0^{\Delta L} F dz = 4EI\left(\frac{n\pi}{L}\right)^2 + \frac{\rho A g \sin\beta}{2R}\left(\frac{L}{n\pi}\right)^2 \tag{A80}$$

The left side of equation (A80) is the work average helical buckling load

$$\overline{F}_{hel} = 4EI\left(\frac{n\pi}{L}\right)^2 + \frac{\rho A g \sin\beta}{2R}\left(\frac{L}{n\pi}\right)^2 \tag{A81}$$

and the right side is the same as equation (A39) given by Dawson and Paslay. Wu and Juvkam-Wold point out that this shows that the critical buckling load given by Dawson and Paslay is actually the average helical buckling load.

The minimum value of $\overline{F}_{hel}$ is found by differentiating it with respect to n, which results in

$$\left(\frac{n\pi}{L}\right)^2 = \sqrt{\frac{\rho Ag \sin\beta}{8EIR}} \tag{A82}$$

Substitution into equation (A81) yields

$$\overline{F}_{hel} = 2\sqrt{2}\left(\frac{\rho AgEI \sin\beta}{R}\right)^{1/2} \tag{A83}$$

For horizontal wellbores $\beta=90°$ and the average helical buckling load is

$$\overline{F}_{hel} = 2\sqrt{2}\left(\frac{\rho AgEI}{R}\right)^{1/2} \tag{A84}$$

Suryanarayana, McCann, Critical Buckling Load

Equation (A71) is a function of n, where n is a continuous positive variable. Differentiation with respect to n yields

$$\frac{dF_{hel(n)}}{dn} = 8EI\frac{\pi^2}{L^2}\left(n - \frac{1}{n^3}\frac{L^4\rho Ag}{8\pi^4 EIR}\right) \tag{A85}$$

and

$$\frac{d^2F_{hel(n)}}{dn^2} = 8EI\frac{\pi^2}{L^2}\left(1 + \frac{3}{n^4}\frac{L^4\rho Ag}{8\pi^4 EIR}\right) \tag{A86}$$

For every $n>0$ equation (A86) is positive; therefore, the graph of $F_{hel(n)}$ versus n is concave upward (see Figure A6).

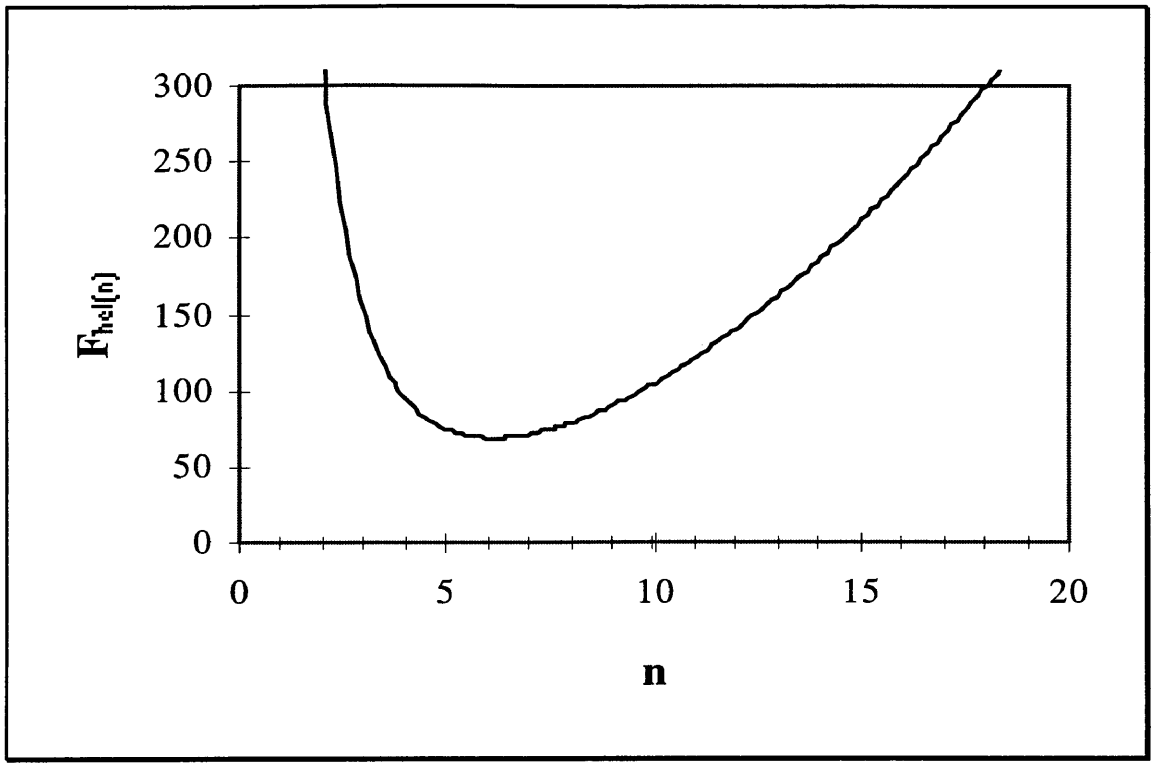

Figure A6. Global minimum of n.

The global minimum at n_O is found when equation (A85) equals zero

$$n_o = \frac{L}{\pi}\left(\frac{\rho A g}{EIR}\right)^{1/4} \tag{A87}$$

APPENDIX B: EXPERIMENTAL APPARATUS

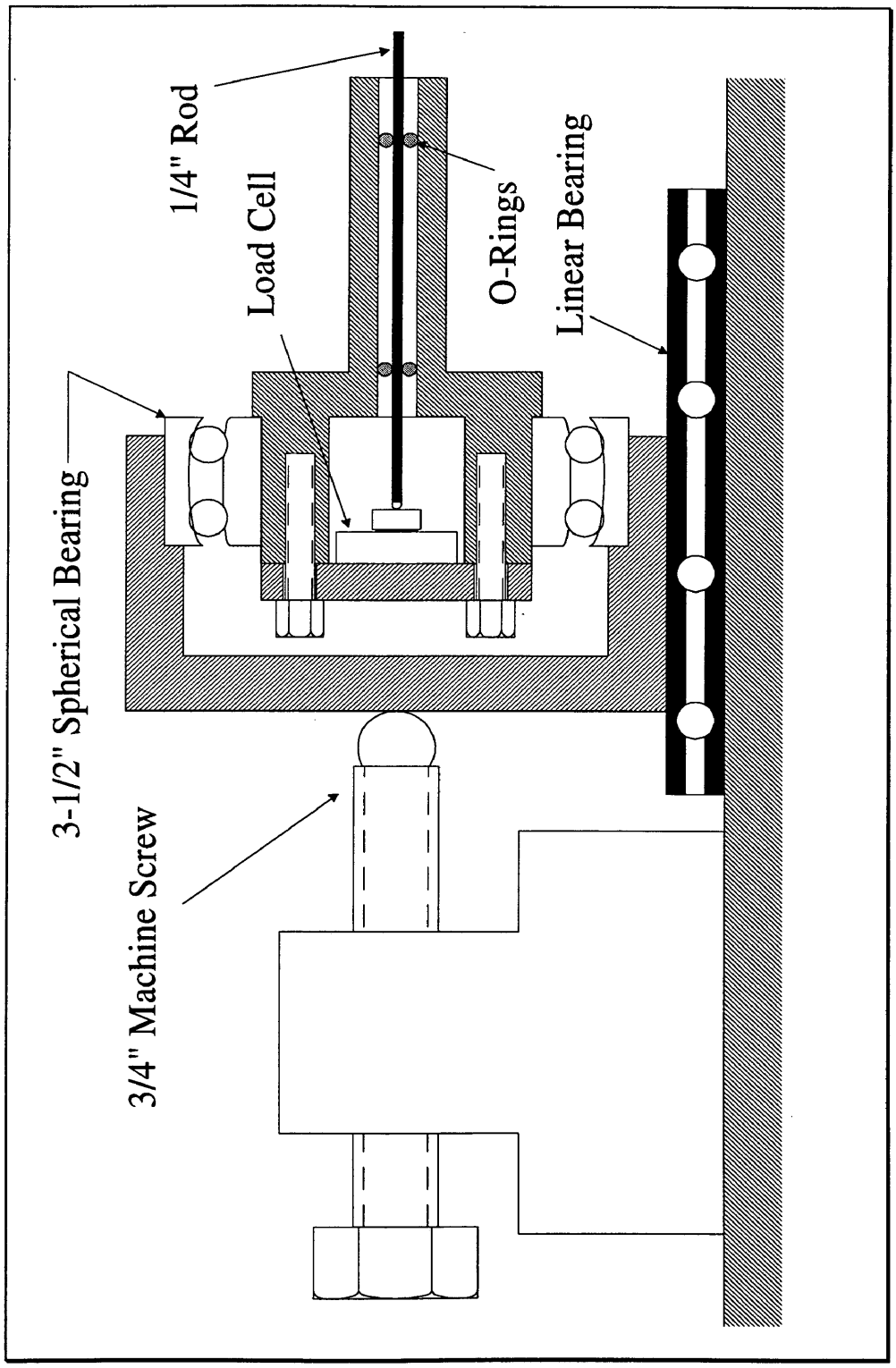

Figure B1. Detail of load cell assembly.

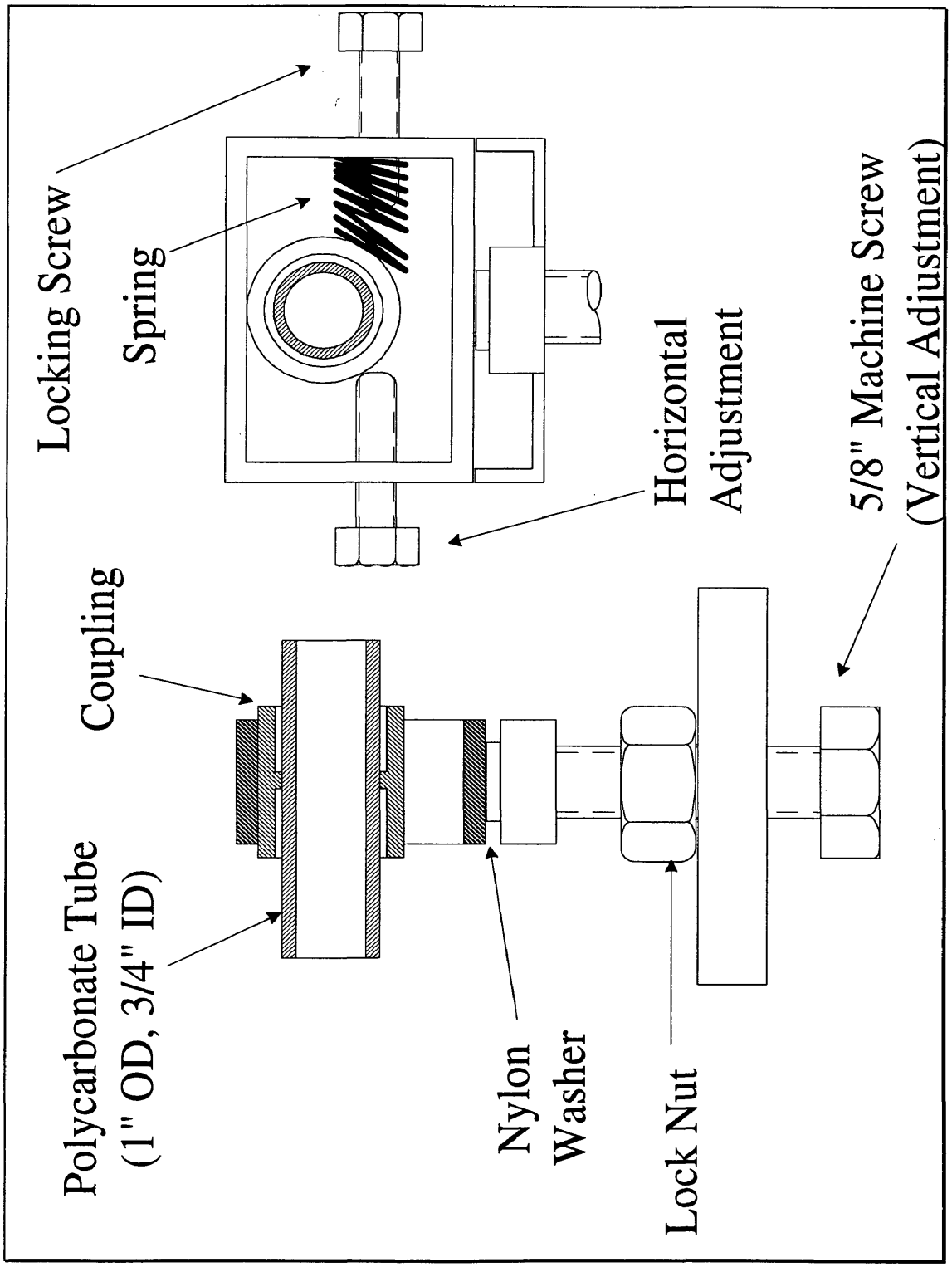

Figure B2. Detail of individual support.

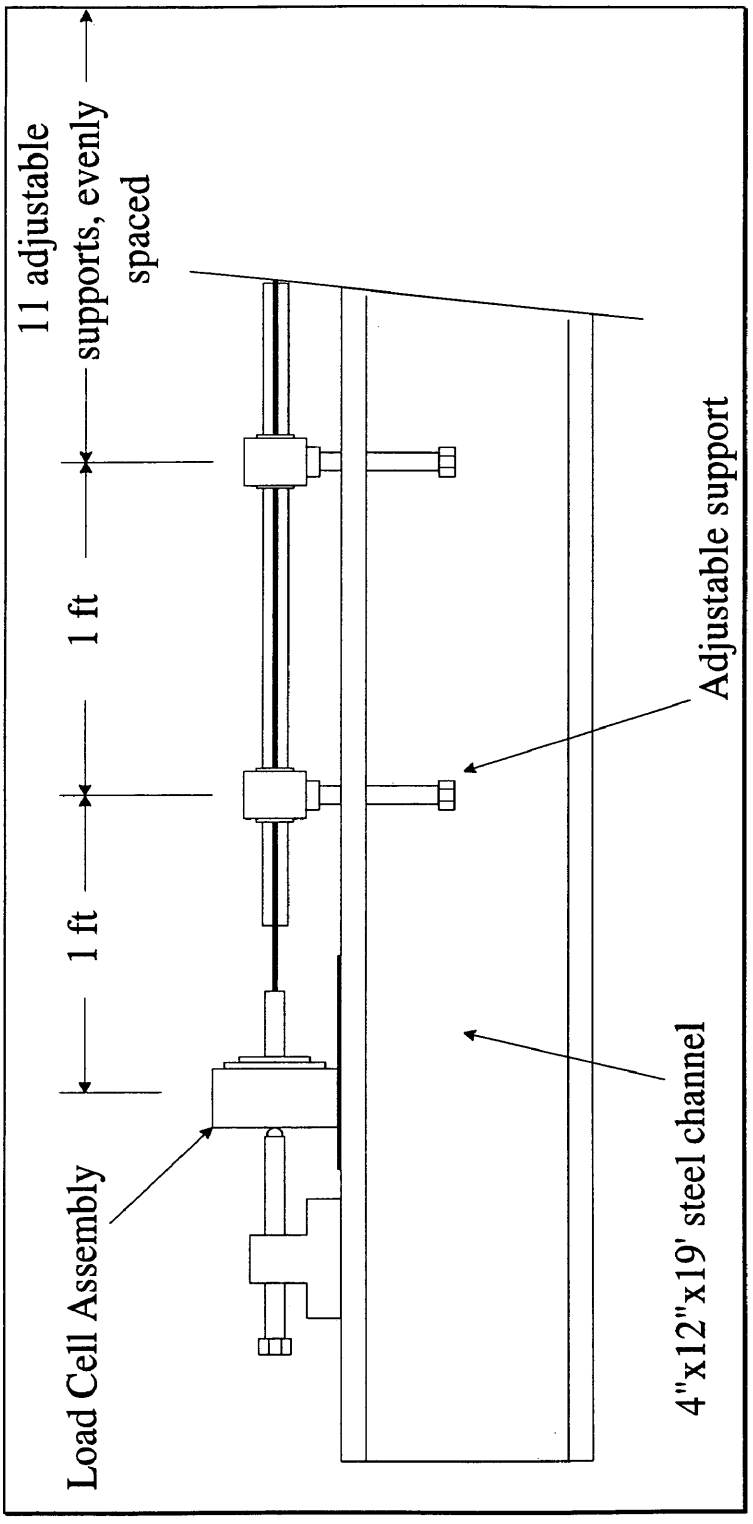

Figure B3. Detail of end assembly.

APPENDIX C: NOMENCLATURE

A	Cross-sectional area of rod
C	Curvature of rod
E	Young's modulus of elasticity
F	Compressional force along helix axis
F_r	Compressional force along rod axis
F_{cr}	Euler critical load
$F_{cr(n)}$	n-th order critical buckling load
$F_{hel(n)}$	n-th order helical buckling load
F_{hel}	helical buckling load
$\overline{F}_{hel}$	Average helical buckling load
g	Gravity
G	Shear modulus of elasticity
I	Moment of inertia of rod
k	Radius of gyration
L	Length of unstressed rod
L_c	Compressed length of rod
L_h	Length of helix measured along helix axis
ΔL	Overall change in rod length
n	order of buckling
p	Pitch
P	Particle arbitrarily close to P_o
P_o	Arbitrary particle in rod
r	Radial spatial coordinate
r_i	Initial radial spatial coordinate
r_r	Radius of rod
R	Radial clearance between rod and hole
$\overline{R}$	Radial distance from center of rod to P_o
s	Length along helix
U	Total potential energy
U_b	Strain energy of bending
U_c	Strain energy of compression

U_f	Potential energy of force F
U_p	Potential energy of helical rod
U_s	Total strain energy
W_f	Work done by force F
W_g	Work done by gravity
α	Angular spatial coordinate
α_i	Initial angular spatial coordinate
θ	Helix angle
ε	Strain
Φ	Angular position of P_o from center of rod
σ	Stress
ρ	Density of rod
υ	Poisson's ratio
ξ	Angular displacement of rod from low side of hole

APPENDIX D: LAB DATA

The following tables show the predetermined heights at which the wellbore supports are placed to establish a given dogleg severity, or radius of curvature.

	Left Load Cell												Right Load Cell
x	-71.2	-60.69	-48.69	-36.75	-24.56	-12.63	0	12.56	23.56	36.06	49.19	61.13	72.7
h	2.5	3.16	3.784	4.269	4.625	4.836	4.911	4.836	4.648	4.293	3.761	3.135	2.5

Table D1. Dogleg severity of 65.33°/100 ft.

	Left Load Cell												Right Load Cell
x	-71.2	-60.69	-48.69	-36.75	-24.56	-12.63	0	12.56	23.56	36.06	49.19	61.13	72.7
h	2.5	2.83	3.141	3.384	3.561	3.667	3.705	3.667	3.573	3.396	3.13	2.817	2.5

Table D2. Dogleg severity of 32.67°/100 ft.

	Left Load Cell												Right Load Cell
x	-71.2	-60.69	-48.69	-36.75	-24.56	-12.63	0	12.56	23.56	36.06	49.19	61.13	72.7
h	2.5	2.5	2.5	2.5	2.5	2.5	2.5	2.5	2.5	2.5	2.5	2.5	2.5

Table D3. Dogleg severity of 0°/100 ft.

The following table shows the data that was taken to calibrate the load cells. Each load cell was fit with a straight line and a second order polynomial. The second order polynomial was used since it was more accurate at lower loads.

	S/N 9318-002	S/N 9318-001
Linear Fit		
Slope	0.14315933	0.1309456
Intercept	-36.9411561	-11.579855
Polynomial Fit		
Power 0	-34.364	-9.25178
Power 1	0.134613	0.119914
Power 2	6.03E-06	9.55E-06

Table D4. Load Cell Fits

	Right Load Cell S/N 9318-002	Left Load Cell S/N 9318-001
Total Load (lb)	millivolts	millivolts
0	246	75
5.1496063	290	121
10.149606	322	158
15.149606	361	202
25.149606	437	275
30.149606	474	316
35.149606	510	354
40.149606	548	401
45.149606	577	442
50.149606	613	486
55.149606	645	520
60.149606	683	564
70.149606	751	633
75.149606	786	673
80.149606	819	713
85.149606	854	754
90.149606	884	766
95.149606	919	805
100.14961	952	842
105.14961	987	881
115.14961	1060	959
120.14961	1097	1000
125.14961	1132	1040
130.14961	1167	1082

Table D5. Load Cell Calibration

The following tables and graphs contain some of the data taken in the experiments.

Left Load Cell		Right Load Cell				
millivolts	Load	millivolts	Load	Displace	ΔL	Comments
78	0.16	248	-0.609	5.067	0	
95	2.226	255	0.354	5.078	0.011	Off bottom 6-10
97	2.47	268	2.145	5.085	0.018	Off bottom 1-6,6-10,1/2 horizontal sine
100	2.835	276	3.248	5.094	0.027	
119	5.153	315	8.637	5.104	0.037	

133	6.866	350	13.49	5.109	0.042	Off bottom 1-11, top 1-4-5, side 6-11
144	8.214	372	16.55	5.115	0.048	
158	9.933	404	21	5.121	0.054	
186	13.38	465	29.53	5.125	0.058	
217	17.22	529	38.53	5.128	0.061	
249	21.2	580	45.74	5.133	0.066	Free 1-2, top 2-4, side 6, top 8-9, side 10, btm 11
290	26.33	651	55.82	5.137	0.07	
336	32.12	715	64.97	5.141	0.074	
387	38.59	794	76.32	5.147	0.08	
442	45.62	861	86.01	5.152	0.085	
489	51.67	928	95.75	5.158	0.091	
557	60.5	1010	107.7	5.164	0.097	Free 1-2, top 2-5, side 6-7, top 8-9, side 10-11
615	68.11	1091	119.7	5.169	0.102	
674	75.91	1166	130.8	5.173	0.106	
692	78.3	1198	135.6	5.175	0.108	
727	82.97	1231	140.5	5.178	0.111	
749	85.92	1266	145.7	5.18	0.113	
782	90.36	1308	152	5.182	0.115	
817	95.09	1364	160.5	5.187	0.12	
466	48.7	963	100.9	5.188	0.121	Loud snap, 1 sine top 2-6, 1 helix 7-11
505	53.74	984	103.9	5.191	0.124	
540	58.29	1013	108.2	5.194	0.127	
573	62.6	1046	113	5.196	0.129	
603	66.53	1075	117.3	5.199	0.132	
653	73.13	1135	126.2	5.203	0.136	
687	77.64	1183	133.3	5.205	0.138	
731	83.51	1229	140.2	5.211	0.144	
583	63.9	1125	124.7	5.214	0.147	Loud snap, 2.5 helix 2-11
650	72.73	1154	129	5.218	0.151	
694	78.57	1184	133.5	5.221	0.154	
728	83.11	1212	137.6	5.225	0.158	
717	81.64	1220	138.8	5.227	0.16	
757	87	1243	142.3	5.23	0.163	
780	90.09	1265	145.6	5.232	0.165	
693	78.44	1241	142	5.229	0.162	
643	71.8	1217	138.4	5.226	0.159	
602	66.4	1195	135.1	5.223	0.156	
574	62.73	1174	132	5.22	0.153	
551	59.72	1156	129.3	5.218	0.151	
516	55.17	1118	123.7	5.215	0.148	
480	50.51	1076	117.5	5.211	0.144	
460	47.93	1045	112.9	5.208	0.141	
428	43.82	992	105.1	5.204	0.137	Same configuratiojn
408	41.26	941	97.64	5.199	0.132	
391	39.09	913	93.56	5.195	0.128	
371	36.55	879	88.62	5.19	0.123	
374	36.93	869	87.17	5.185	0.118	Free 5
359	35.03	847	83.98	5.182	0.115	
325	30.73	798	76.9	5.177	0.11	
314	29.34	767	72.43	5.174	0.107	
309	28.71	763	71.85	5.171	0.104	1 sine 2-6, 1 helix 6-11
305	28.21	756	70.85	5.167	0.1	
295	26.95	742	68.84	5.162	0.095	2.5 sine 2-11
292	26.58	732	67.4	5.158	0.091	
269	23.7	688	61.1	5.153	0.086	
246	20.83	644	54.83	5.15	0.083	
237	19.7	625	52.12	5.146	0.079	
215	16.97	590	47.16	5.141	0.074	Free 1, top 2-9, free 10-11
198	14.87	562	43.19	5.138	0.071	
182	12.89	533	39.1	5.136	0.069	
160	10.18	490	33.04	5.132	0.065	
152	9.196	468	29.96	5.131	0.064	
141	7.846	443	26.45	5.129	0.062	1 sine top 2-10
128	6.254	407	21.42	5.127	0.06	
124	5.764	395	19.75	5.125	0.058	
122	5.52	389	18.91	5.123	0.056	
119	5.153	382	17.94	5.121	0.054	
119	5.153	377	17.24	5.12	0.053	Free 1-2, top 2-9, Free 10-11

108	3.81	348	13.21	5.117	0.05	
105	3.445	334	11.27	5.114	0.047	
100	2.835	317	8.914	5.11	0.043	Free 1-3, top 2-9, free 10-11
97	2.47	307	7.53	5.108	0.041	
94	2.105	301	6.701	5.106	0.039	Free 1-4, 1:00 5-9, free 10-11
92	1.861	296	6.01	5.103	0.036	
93	1.983	294	5.733	5.1	0.033	free 1-5, side 6-10
91	1.739	290	5.181	5.096	0.029	
90	1.618	288	4.904	5.094	0.027	
88	1.375	283	4.214	5.091	0.024	
85	1.01	275	3.11	5.088	0.021	
84	0.888	271	2.559	5.086	0.019	
79	0.281	260	1.043	5.082	0.015	

Table D6. Experimental data for 65°/100 ft.

Left Load Cell		Right Load Cell				
millivolts	Load	millivolts	Load	Displ	ΔL	Comments
78	0.16	254	0.217	5.081	0	
91	1.739	281	3.938	5.088	0.007	
99	2.713	294	5.733	5.098	0.017	off btm 1-5, side 6-10
101	2.957	299	6.424	5.104	0.023	
114	4.543	332	10.99	5.11	0.029	top 2-5, side 5-10
131	6.621	375	16.96	5.115	0.034	
135	7.111	382	17.94	5.119	0.038	
140	7.723	396	19.89	5.123	0.042	
195	14.49	500	34.45	5.131	0.05	
247	20.95	591	47.3	5.137	0.056	top 2-5, side 6-7, top 7-9, side 10-11
286	25.82	651	55.82	5.14	0.059	
323	30.48	710	64.25	5.145	0.064	
366	35.92	764	72	5.149	0.068	
402	40.5	816	79.49	5.152	0.071	
449	46.52	880	88.76	5.157	0.076	
501	53.22	947	98.52	5.162	0.081	top 2-4, 1.5 sine 4-11, 1:00
567	61.81	1030	110.7	5.167	0.086	
588	64.56	1068	116.3	5.169	0.088	
667	74.98	1158	129.6	5.174	0.093	
695	78.7	1194	135	5.177	0.096	
744	85.25	1259	144.7	5.182	0.101	
435	44.72	913	93.56	5.184	0.103	Loud snap, 1 sine 2-6, 1+ helix 6-11
531	57.12	987	104.4	5.19	0.109	
608	67.19	1071	116.7	5.195	0.114	
671	75.51	1148	128.1	5.202	0.121	
720	82.04	1199	135.7	5.205	0.124	
727	82.97	1234	140.9	5.21	0.129	
732	83.64	1245	142.6	5.214	0.133	
794	91.98	1274	146.9	5.218	0.137	
605	66.79	1140	126.9	5.219	0.138	loud snap, 2.5 helix 2-11
702	79.64	1187	133.9	5.226	0.145	
763	87.8	1236	141.2	5.231	0.15	
834	97.4	1300	150.8	5.237	0.156	
775	89.42	1282	148.1	5.24	0.159	soft snap, 2.5 helix 2-11
845	98.9	1317	153.4	5.245	0.164	
878	103.4	1346	157.7	5.248	0.167	
745	85.39	1305	151.6	5.242	0.161	
637	71.01	1248	143	5.235	0.154	
550	59.59	1168	131.1	5.227	0.146	
500	53.09	1098	120.7	5.221	0.14	2.5 helix, tighter at right
470	49.22	1045	112.9	5.216	0.135	
429	43.95	975	102.6	5.208	0.127	
402	40.5	926	95.46	5.202	0.121	
387	38.59	899	91.52	5.198	0.117	
372	36.68	863	86.3	5.188	0.107	1 sine top 2-6, 1.5 helix 6-11
323	30.48	782	74.59	5.18	0.099	
304	28.08	750	69.99	5.174	0.093	
301	27.71	735	67.83	5.168	0.087	1.5 sine 2-7, free 7-9, .5 sine 9-11
281	25.2	701	62.96	5.16	0.079	

270	23.82	685	60.67	5.153	0.072	free 1-2, 2.5 sine 2-11, higher amp 6-11
216	17.1	595	47.86	5.146	0.065	
185	13.26	536	39.52	5.139	0.058	
158	9.933	482	31.92	5.133	0.052	free 1-2, top 2-9, side 9-11
137	7.356	428	24.35	5.13	0.049	
120	5.275	387	18.63	5.124	0.043	
109	3.932	350	13.49	5.119	0.038	
102	3.079	329	10.58	5.115	0.034	
96	2.348	309	7.807	5.11	0.029	free 1-3, top 3-9, side 9-11
91	1.739	297	6.148	5.106	0.025	
93	1.983	294	5.733	5.1	0.019	free 1-5, side 5-10
91	1.739	290	5.181	5.095	0.014	
89	1.496	284	4.352	5.092	0.011	
78	0.16	258	0.767	5.084	0.003	

Table D7. Experimental data for 65°/100 ft.

Left Load Cell		Right Load Cell				
millivolts	Load	millivolts	Load	Displ	ΔL	Comments
80	0.402	253	0.079	5.062	0	
105	3.445	307	7.53	5.074	0.012	
116	4.787	336	11.55	5.085	0.023	off btm 1-6
139	7.601	385	18.36	5.093	0.031	free 1-3, top 3-4, side 5-9 btm 9-11
175	12.03	460	28.83	5.101	0.039	
180	12.64	473	30.66	5.108	0.046	
230	18.83	555	42.2	5.116	0.054	free 1-2, top 2, .5 helix 2-6, free 6-7, .5 helix 7-11
297	27.21	650	55.68	5.12	0.058	
400	40.24	791	75.89	5.128	0.066	
494	52.32	910	93.13	5.134	0.072	
574	62.73	1016	108.6	5.14	0.078	2 helix 1-11, tighter at right
641	71.54	1095	120.3	5.145	0.083	
693	78.44	1165	130.6	5.149	0.087	
832	97.13	1333	155.8	5.16	0.098	
927	110.1	1466	175.9	5.168	0.106	
998	119.9	1556	189.7	5.171	0.109	
1044	126.3	1626	200.5	5.177	0.115	1.5 helix 2-11, reversal 2
815	94.82	1471	176.7	5.179	0.117	snap, 1.5 helix 3-11, reversal 3
899	106.3	1502	181.4	5.183	0.121	
969	115.9	1550	188.8	5.187	0.125	
1067	129.6	1642	202.9	5.194	0.132	
1156	142.1	1756	220.6	5.201	0.139	reversal moved from 12:00 to 9:00
716	81.5	1321	154	5.204	0.142	loud snap, 1 helix 1-4, reversal 5, 1 helix 5-11
818	95.23	1376	162.3	5.211	0.149	
883	104.1	1436	171.4	5.217	0.155	
942	112.2	1494	180.2	5.222	0.16	
918	108.9	1491	179.7	5.225	0.163	soft snap, reversal 5, tighter helixes near center
945	112.6	1571	192	5.234	0.172	
770	88.75	1494	180.2	5.224	0.162	
675	76.04	1375	162.1	5.213	0.151	
609	67.32	1279	147.7	5.205	0.143	
547	59.2	1169	131.2	5.197	0.135	
519	55.56	1130	125.4	5.191	0.129	still reversed at 5
486	51.28	1058	114.8	5.184	0.122	
453	47.03	997	105.8	5.177	0.115	
450	46.64	965	101.2	5.173	0.111	loud snap, almost 3 helixes 1-11
350	33.89	834	82.1	5.166	0.104	
302	27.83	750	69.99	5.156	0.094	2.5 helix 1-11
322	30.35	761	71.57	5.146	0.084	1 sine 2-6, 1.5 helix 6-11
271	23.95	707	63.82	5.139	0.077	
226	18.34	631	52.98	5.132	0.07	1 sine 2-6, 1 helix 6-11
188	13.63	549	41.36	5.125	0.063	
171	11.53	509	35.72	5.119	0.057	
146	8.459	453	27.85	5.112	0.05	free 1-3, top 3-4, free 5-6, .5 helix 6-10, free 10-11
136	7.233	430	24.63	5.107	0.045	
118	5.031	391	19.19	5.102	0.04	free 1-3, 2:00 3-5, free 5-7, 10:00 7-9, free 9-11
113	4.42	367	15.85	5.098	0.036	
104	3.323	342	12.38	5.091	0.029	

99	2.713	328	10.44	5.087	0.025	
88	1.375	289	5.043	5.082	0.02	
81	0.524	263	1.456	5.076	0.014	
77	0.038	255	0.354	5.074	0.012	

Table D8. Experimental data for 33°/100 ft.

Left Load Cell		Right Load Cell				
millivolts	Load	millivolts	Load	Displ	ΔL	Comments
78	0.16	256	0.492	5.066	0	
100	2.835	295	5.871	5.072	0.006	
148	8.705	399	20.31	5.077	0.011	
165	10.79	435	25.33	5.079	0.013	
199	14.99	506	35.29	5.082	0.016	5:00 at 9-10
205	15.73	517	36.84	5.087	0.021	
234	19.33	569	44.18	5.09	0.024	2 sine 1-11
200	15.11	523	37.69	5.096	0.03	
231	18.96	566	43.76	5.098	0.032	1 sine 1-6, 1 helix 6-11
270	23.82	619	51.27	5.101	0.035	
308	28.59	675	59.25	5.104	0.038	sine wave climbing south side
365	35.79	759	71.28	5.107	0.041	
427	43.69	835	82.24	5.109	0.043	
495	52.45	925	95.31	5.113	0.047	
583	63.9	1039	112	5.121	0.055	
586	64.3	1049	113.5	5.121	0.055	soft snap, sine wave climbed up to 1:00
668	75.11	1136	126.3	5.128	0.062	
717	81.64	1193	134.8	5.13	0.064	
787	91.04	1287	148.9	5.134	0.068	
861	101.1	1376	162.3	5.138	0.072	
917	108.7	1451	173.6	5.145	0.079	
944	112.5	1475	177.3	5.148	0.082	
962	114.9	1517	183.7	5.155	0.089	.5 helix 1-4, 1.5 helix 4-11
1017	122.6	1579	193.2	5.162	0.096	
1073	130.4	1641	202.8	5.169	0.103	
1125	137.7	1693	210.8	5.172	0.106	
917	108.7	1608	197.7	5.168	0.102	
834	97.4	1532	186	5.162	0.096	still reversed 4
764	87.94	1440	172	5.154	0.088	
682	76.97	1326	154.7	5.145	0.079	
609	67.32	1222	139.1	5.14	0.074	
531	57.12	1105	121.7	5.134	0.068	
449	46.52	975	102.6	5.127	0.061	
357	34.77	845	83.69	5.122	0.056	snap, 2 helix 1-11 same pitch throughout
286	25.82	729	66.97	5.115	0.049	
242	20.33	657	56.68	5.111	0.045	
187	13.51	551	41.64	5.106	0.04	
155	9.564	484	32.2	5.1	0.034	
144	8.214	455	28.13	5.091	0.025	
130	6.498	423	23.66	5.087	0.021	2 sine 1-11 5:00
115	4.665	380	17.66	5.083	0.017	
102	3.079	340	12.1	5.081	0.015	
87	1.253	284	4.352	5.077	0.011	
77	0.038	257	0.63	5.073	0.007	

Table D9. Experimental data for 0°/100 ft.

Left Load Cell		Right Load Cell				
millivolts	Load	millivolts	Load	Displ	ΔL	Comments
80	0.402	253	0.079	5.068	0	
83	0.767	254	0.217	5.07	0.002	
86	1.131	257	0.63	5.073	0.005	
88	1.375	259	0.905	5.075	0.007	
89	1.496	263	1.456	5.076	0.008	
95	2.226	279	3.662	5.076	0.008	
98	2.592	288	4.904	5.077	0.009	.5 sine 1-11
107	3.688	309	7.807	5.078	0.01	
117	4.909	333	11.13	5.079	0.011	

128	6.254	358	14.6	5.08	0.012	
140	7.723	391	19.19	5.081	0.013	
167	11.04	453	27.85	5.084	0.016	
175	12.03	469	30.1	5.085	0.017	
181	12.77	483	32.06	5.088	0.02	1.5 sine 1-11
190	13.88	496	33.89	5.088	0.02	
194	14.37	502	34.73	5.09	0.022	
207	15.98	526	38.11	5.092	0.024	
224	18.09	553	41.92	5.093	0.025	
222	17.84	554	42.06	5.094	0.026	
165	10.79	477	31.22	5.096	0.028	
180	12.64	496	33.89	5.098	0.03	reversal 4, 1 helix 6-11
203	15.48	525	37.97	5.099	0.031	
238	19.83	575	45.03	5.102	0.034	
269	23.7	614	50.56	5.104	0.036	
213	16.72	569	44.18	5.102	0.034	
188	13.63	533	39.1	5.1	0.032	
175	12.03	509	35.72	5.098	0.03	
160	10.18	486	32.48	5.097	0.029	
151	9.073	464	29.39	5.095	0.027	
145	8.337	447	27.01	5.093	0.025	
146	8.459	446	26.87	5.091	0.023	
139	7.601	437	25.61	5.091	0.023	
133	6.866	421	23.38	5.088	0.02	high amp sine 1-11
132	6.743	415	22.54	5.087	0.019	
129	6.376	406	21.28	5.085	0.017	
126	6.009	399	20.31	5.085	0.017	
123	5.642	392	19.33	5.084	0.016	
127	6.131	389	18.91	5.083	0.015	
119	5.153	375	16.96	5.082	0.014	
115	4.665	368	15.99	5.082	0.014	
112	4.298	356	14.32	5.081	0.013	
109	3.932	349	13.35	5.08	0.012	
104	3.323	331	10.85	5.079	0.011	
101	2.957	323	9.745	5.079	0.011	
97	2.47	311	8.084	5.078	0.01	
93	1.983	297	6.148	5.077	0.009	
89	1.496	284	4.352	5.077	0.009	
86	1.131	274	2.972	5.076	0.008	
85	1.01	270	2.421	5.076	0.008	
82	0.645	264	1.594	5.075	0.007	
81	0.524	257	0.63	5.075	0.006	
81	0.524	255	0.354	5.074	0.006	
80	0.402	255	0.354	5.073	0.005	

Table D10. Experimental data for 0°/100 ft.

Left Load Cell		Right Load Cell				
millivolts	Load	millivolts	Load	Displ	ΔL	Comments
79	0.281	252	-0.059	5.078	0	
82	0.645	252	-0.059	5.081	0.003	
82	0.645	252	-0.059	5.083	0.005	
87	1.253	261	1.181	5.084	0.006	
87	1.253	264	1.594	5.086	0.008	
91	1.739	278	3.524	5.088	0.01	
92	1.861	281	3.938	5.088	0.011	
92	1.861	283	4.214	5.089	0.012	
92	1.861	284	4.352	5.09	0.013	
93	1.983	284	4.352	5.091	0.013	
93	1.983	284	4.352	5.091	0.014	
94	2.105	286	4.628	5.092	0.014	
94	2.105	287	4.766	5.092	0.015	
94	2.105	288	4.904	5.093	0.015	
96	2.348	290	5.181	5.094	0.016	
96	2.348	293	5.595	5.094	0.017	
96	2.348	295	5.871	5.095	0.017	
98	2.592	297	6.148	5.095	0.018	

98	2.592	301	6.701	5.096	0.019	
101	2.957	306	7.392	5.097	0.02	
102	3.079	310	7.945	5.098	0.02	
104	3.323	313	8.36	5.098	0.021	
103	3.201	314	8.499	5.099	0.021	
103	3.201	316	8.776	5.1	0.023	
102	3.079	316	8.776	5.101	0.024	
104	3.323	318	9.052	5.102	0.024	
106	3.566	319	9.191	5.102	0.025	
106	3.566	323	9.745	5.103	0.026	
106	3.566	326	10.16	5.104	0.026	
110	4.054	332	10.99	5.104	0.027	
108	3.81	330	10.71	5.106	0.028	off btm 1-6
109	3.932	333	11.13	5.107	0.029	
113	4.42	341	12.24	5.108	0.03	
118	5.031	350	13.49	5.109	0.031	
122	5.52	361	15.02	5.109	0.032	
118	5.031	359	14.74	5.11	0.033	
126	6.009	370	16.27	5.111	0.034	
130	6.498	379	17.52	5.112	0.034	
136	7.233	393	19.47	5.112	0.035	
138	7.478	398	20.17	5.113	0.035	
138	7.478	401	20.59	5.113	0.036	
144	8.214	409	21.7	5.114	0.037	
144	8.214	415	22.54	5.115	0.038	
148	8.705	420	23.24	5.116	0.039	
152	9.196	427	24.21	5.117	0.04	
157	9.81	436	25.47	5.118	0.04	
160	10.18	444	26.59	5.118	0.041	
162	10.42	450	27.43	5.12	0.042	

Table D11. Experimental data for 33°/100 ft.

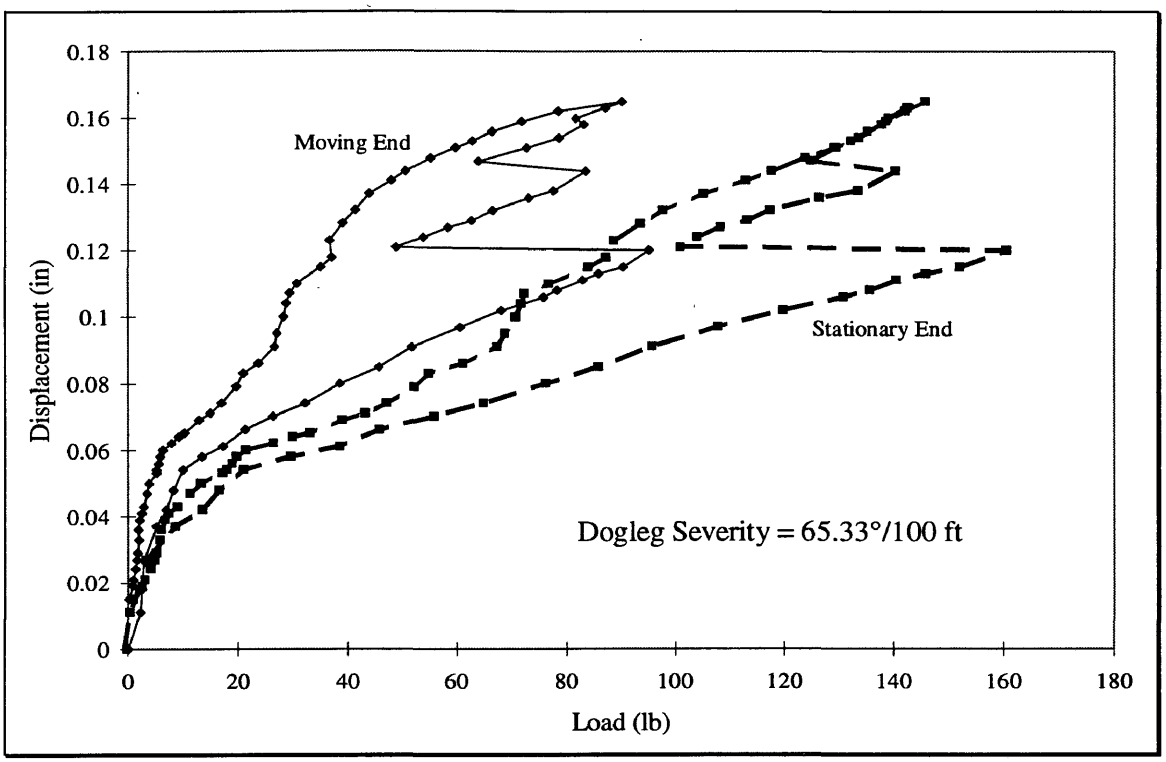

Figure D1. Stationary load/moving load comparison for 65°/100 ft.

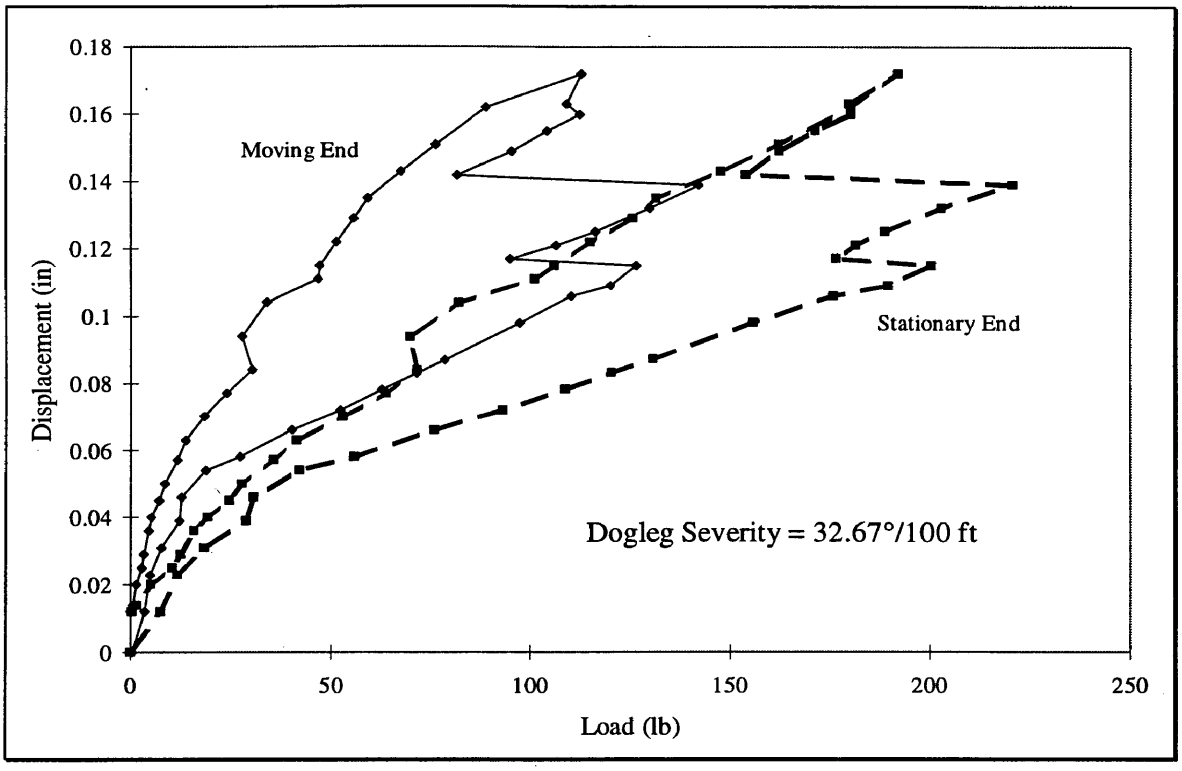

Figure D2. Stationary load/moving load comparison for 33°/100 ft.

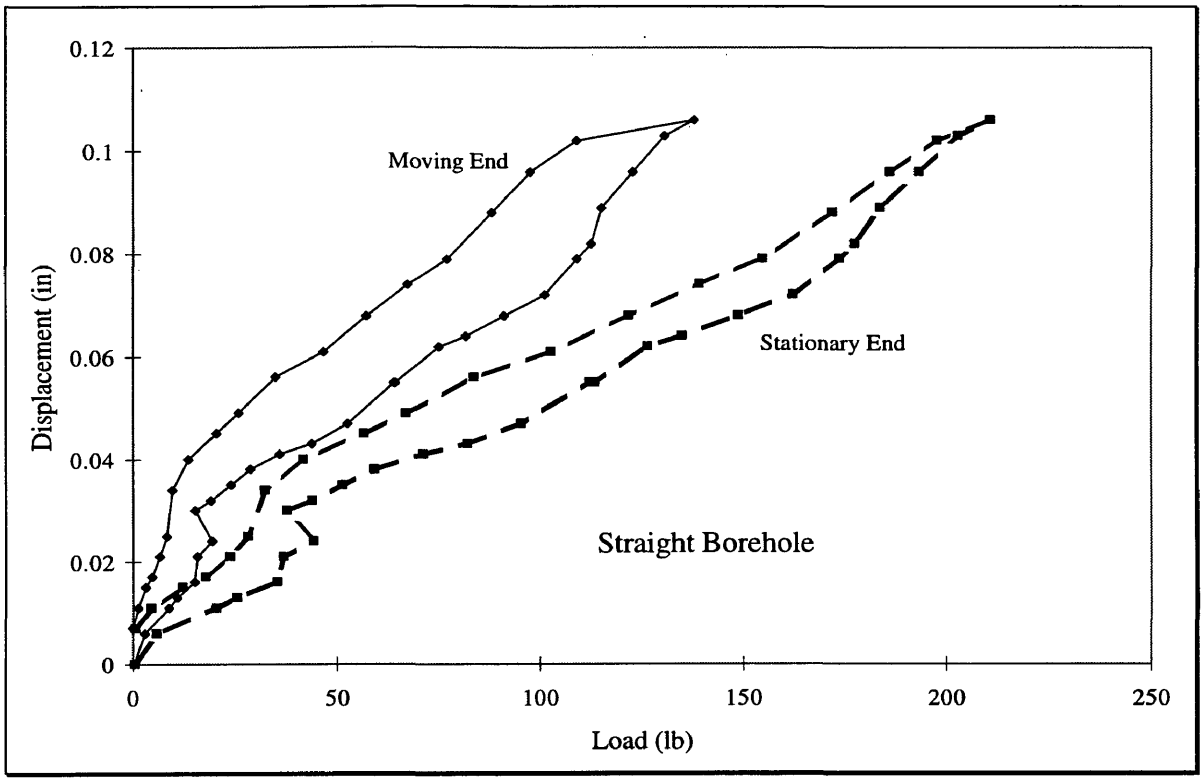

Figure D3. Stationary load/moving load comparison for straight borehole.

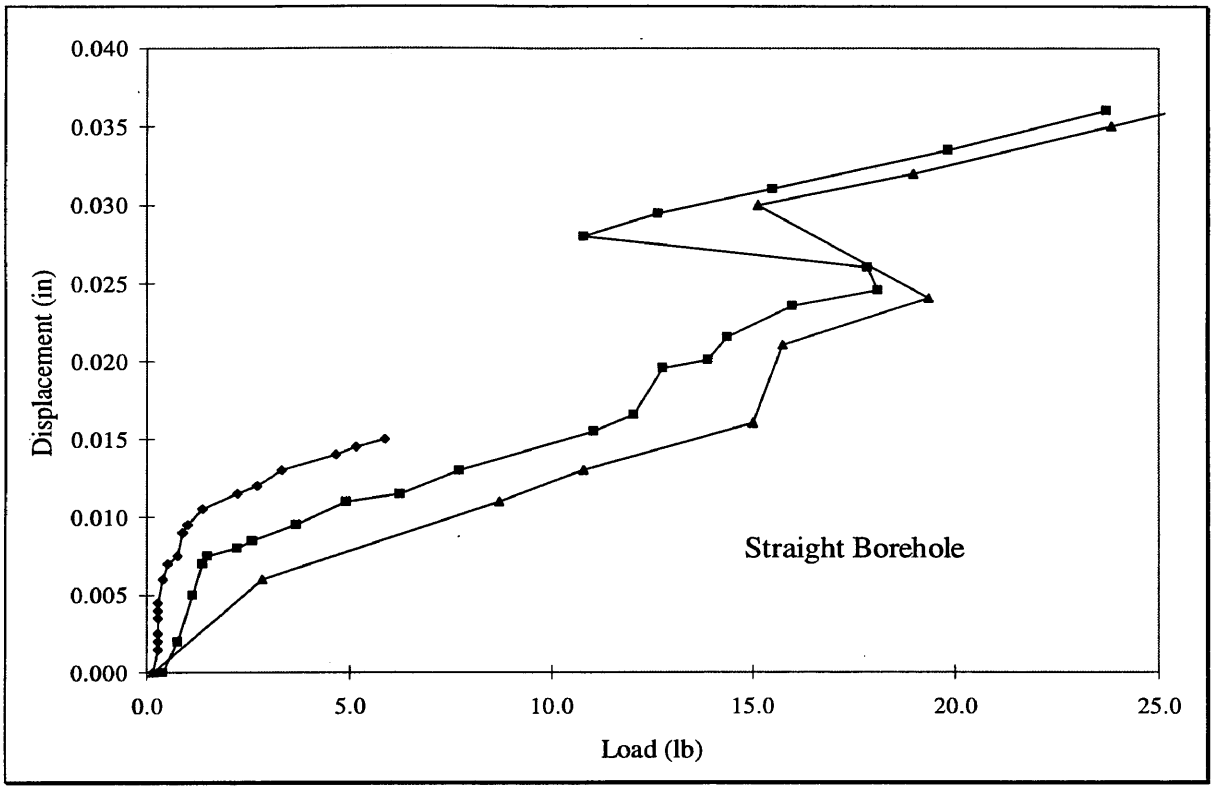

Figure D4. Repeatability of data from straight borehole (loading only).

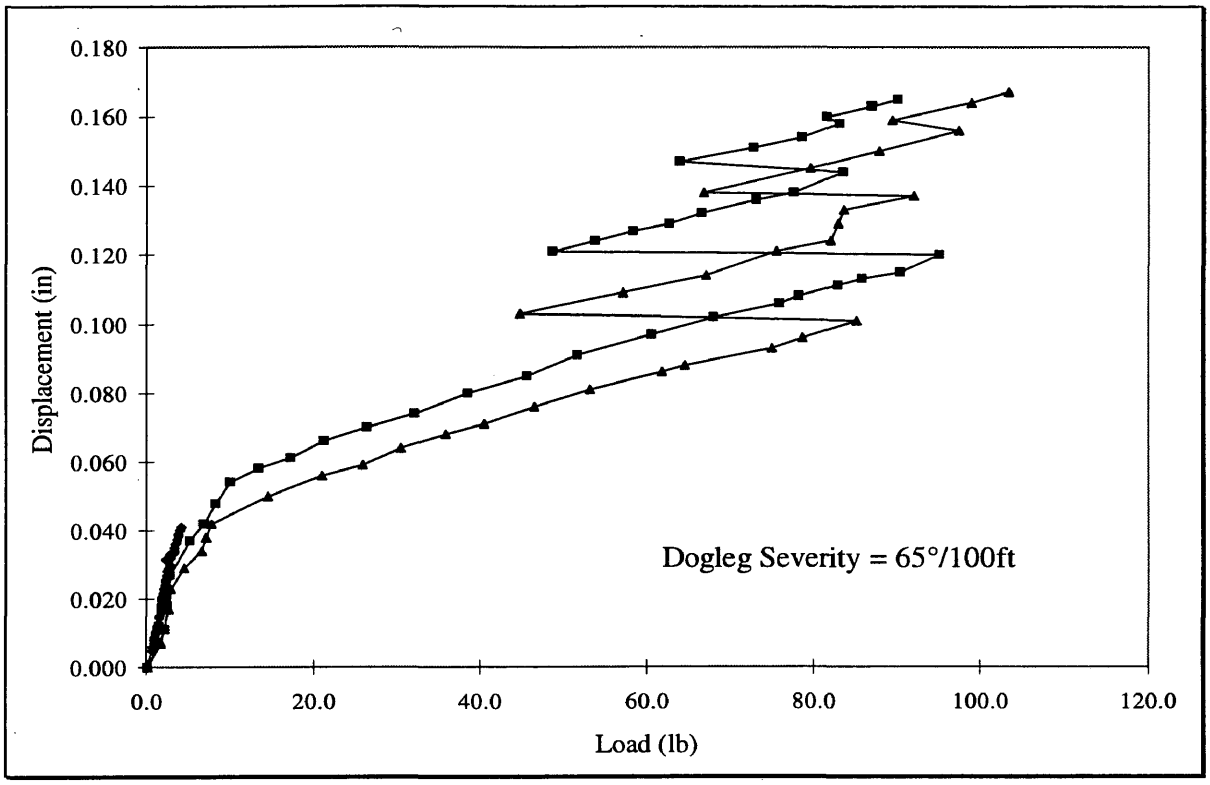

Figure D5. Repeatability of data from 65°/100 ft borehole (loading only).

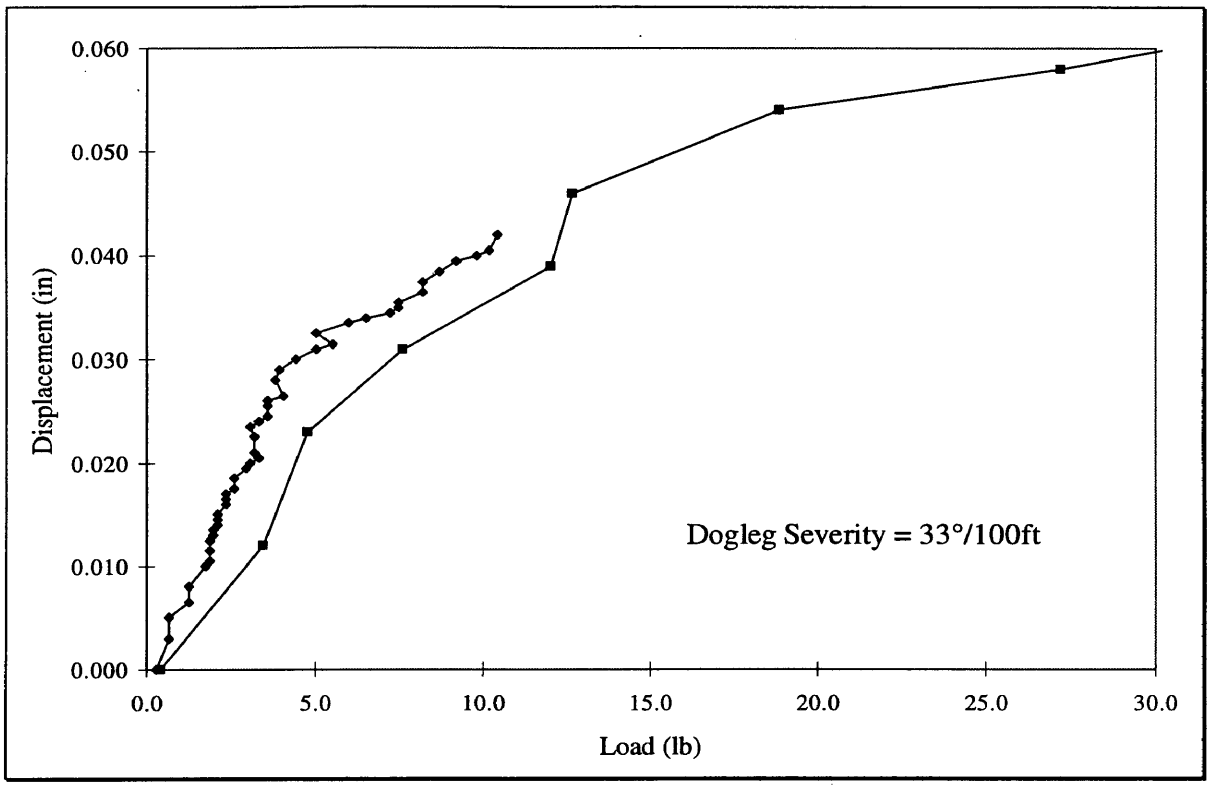

Figure D6. Repeatability of data from 33°/100 ft borehole (loading only).